arXiv:1703.04246v1 [nlin.PS] 13 Mar 2017

Control of traveling localized spots

S. Martens[1], C. Ryll[2], J. Löber[1], F. Tröltzsch[2], H. Engel[1]

[1] Institut für Theoretische Physik, Hardenbergstraße 36, EW 7-1, Technische Universität Berlin, 10623 Berlin, Germany
[2] Technische Universität Berlin, Institut für Mathematik, 10623 Berlin, Germany

E-mail: steffen.martens@tu-berlin.de

Abstract. The ability to control a desired dynamics or pattern in reaction-diffusion systems has attracted considerable attention over the last decades and it is still a fundamental problem in applied nonlinear science. Besides traveling waves, moving localized spots – also called dissipative solitons – represent yet another important class of self-organized spatio-temporal structures in non-equilibrium dissipative systems. In this work, we focus attention to control aspects and present an efficient method to control both the position and orientation of these moving localized structures according to a prescribed protocol of movement. In detail, we present two different approaches to guide a localized spot along a pre-given trajectory. First, an analytical solution for the control – being an open-loop control – is proposed which attempts to shift the spot without disturbing its profile. The control signal is expressed in terms of the uncontrolled spot profile and its propagation velocity; rendering detailed informations about the reaction kinetics unnecessary. Secondly, the standard formulation of optimal control with an objective functional involving the Tikhonov regularization is used. We confirm, within numerical accuracy, that the analytical position control is indeed the solution to an unregularized optimal control problem and even close to the regularized one. Consequently, the analytic expressions are excellent initial guesses for the numerical calculation of regularized optimal control problems, thereby achieving a substantial computational speedup.

PACS numbers: 82.40.Ck, 02.30.Yy, 82.40.Bj

Submitted to: *New J. Phys.*

Introduction

Reaction-diffusion systems (RDS) model phenomena from a large variety of fields including chemical systems [1], information processing in nervous systems [2], coordination of heart beat [3], spatial spread of diseases [4], cell dynamics [5], and motility of crawling cells [6, 7, 8], to name only a few. These systems possess a rich variety of solutions ranging from homogeneous stable steady states, phase waves, Turing patterns, stationary localized and labyrinthine patterns, traveling, rotating, and scroll waves to fully developed spatio-temporal turbulence [9, 10].

The ability to control a desired dynamics or pattern in RDS has attracted considerable attention over the last decades [11, 12] and it is still a challenging and fundamental problem in applied nonlinear science. Several control strategies have been developed for purposeful manipulation of RDS as, e.g., the application of feedback-mediated control loops (closed-loops) with and without delays [13, 14, 15] and open-loop control. The latter includes external spatial distributed forcing [16, 17], localized forcing by point actuators [18, 19], optimal control [20, 21, 22], and control by imposed geometric constraints [23, 24, 25] and heterogeneities on the medium [26, 27].

A particularly simple but still general control task is *position control* of traveling waves. In position control, the location as well as the orientation of a desired traveling wave is guided according to a prescribed trajectory in space in order to e.g. avoid direct contact of the controlled pattern with the domain boundaries or local heterogeneities inside the medium. Simultaneously, the wave profile is kept as close as feasible to the uncontrolled traveling waves profile. Note that position control is intimately connected with the symmetries of the system's Euclidean domain, e.g., two translational and one rotational degrees of freedom in a two-dimensional spatial domain.

An experimental example of open loop position control is the guidance of traveling CO pulses on an addressable catalytic surface by a computer controlled, focused laser beam [28]. Thereby, the averaged reaction rate is significantly enhanced by a given speed of the moving laser spot [29]. Controlling the excitability of a photosensitive Belousov-Zhabotinsky (BZ) medium [11] by temporally periodic changing of the applied, spatially homogeneous light intensity forces a spiral wave tip to describe a wide range of hypocycloidal and epicycloidal trajectories [30, 31]. An open loop scheme similarly aiming at the position of wave patterns is the light controlled interface dynamics in an optical bistable medium [32]. Theoretical studies of dragging one-dimensional chemical fronts or phase interfaces by anchoring the latter to a movable parameter heterogeneity can be found in [33].

Position control can be tackled by feedback control as well. In experiments with spiral waves in the BZ reaction, the spiral wave core is steered around obstacles using feedback signals obtained from wave activity measured at detector points, along detector lines, or in a spatially extended control domain [16, 34, 35]. Two feedback loops were used to guide wave segments along pre-given trajectories [36]. Furthermore, feedback-mediated control loops are employed to stabilize e.g. unstable steady states [37], unstable traveling wave segments [38], or rigidly rotating unstable spiral waves in the regime of stable meandering spiral waves [39].

Despite the large number of successfully applied controls in experiments, these schemes possess disadvantages as well. For example, feedback control necessitates continuous monitoring of the system. Moreover, the presence of time-delayed feedback can induce complex spatial-temporal behavior to localized wave patterns, including the formation of target patterns, spontaneous motion, spontaneous breathing, and

various complex structures resulting from multimode oscillatory instabilities [40, 41]. On the other hand, open-loop control is based on a detailed knowledge of the system's dynamics and is inherent instable against perturbations of the initial conditions as well as other data uncertainty. While both approaches have been successfully applied to reaction-diffusion systems and hence have received much attention, optimal control of RDS remains largely unexplored [22, 42, 43], at least within the physics community. One reason might lie in the requirement of complete knowledge of the underlying partial differential equations (PDEs) governing the systems evolution in time and space as well as the associated system parameters. Additionally, the numerical solution of optimal control problems is computationally expensive restricting the calculations to comparably small spatial domains and short time intervals. Even worse, optimal feedback control of PDEs becomes almost intractable [44]. In view of the numerical difficulties, analytical approaches have some benefits and might be used to obtain solutions to optimal control for a number of systems with relative ease.

Recently, we've proposed an novel position control that guide a traveling wave over time according to a prescribed *protocol of motion* while preserving simultaneously the wave profile [45]. Without knowledge of the nonlinear reaction kinetics and the system parameters, we've derived analytically the control realizing the given protocol of motion. Intriguingly, this control is close to the solution of a corresponding unregularized optimal control problem [46]. Further, an extension of the proposed control allows the investigation of the stability of controlled traveling waves [47], which can never be taken for granted in open loop control systems. Moreover, a modification of the method provides shaping of wave patterns in two-dimensional RDS by shifting the position of a trajectory outlining the pattern [48]. Further, an extension of the proposed control allows the investigation of the stability of controlled traveling waves [47], which can never be taken for granted in open loop control systems. In two spatial dimension, also the shape of traveling reaction-diffusion waves was successfully controlled by our method [48].

In previous work, we applied analytical position control to one-dimensional traveling chemical fronts and excitation pulses [45, 46, 49]. These traveling waves are "building blocks" of wave segments and spiral waves as well as more complex scroll waves in two and three spatial dimensions, respectively. In the work at hand, we extend our method to position control of spatially localized moving spots in two spatial dimensions. These self-organized localized patterns have been studied in various RDS ranging from gas-discharge systems [50], optics and laser physics [51], actin conformations in dicty [52], neural activity in head-direction cells [53], vegetation patterns [54] to structureless memory devices [55, 56]. Spots turned out to be of particular interest for fundamental studies as well as for applications (see, e.g., [57, 58] and references thereafter). Appearing in non-equilibrium dissipative systems, they are often referred to as dissipative solitons [50]; other frequently used terminology includes autosolitons, bumps or shortly spots.

While the interaction of localized spots with heterogeneities and their interaction among each other have been widely investigated While the particle-like features of localized spot solutions and their interaction among each other have been widely investigated [59, 60], position control of these patterns have not attract much attention yet. First, we shortly introduce the studied three-component reaction-diffusion model in section 1. In section 2.1, we present our analytical approach for the position control of RD patterns in fully actuated systems. These analytical controls are solutions to the unregularized optimal control problem. The standard formulation of optimal control

with an objective functional involving the Tikohonov regularization is stated explicitly in section 2.2. Section 3 is dedicated to a brief description of the numerical methods being used, followed by a discussion of numerical examples; namely, position without orientation control 3.1, orientation control 3.3, and position control by a single control signal 3.4. Finally, we conclude the results in section 4.

1. Three-component spot model

We study position control of traveling localized patterns by means of the following three-component reaction-diffusion (RD) system

$$\partial_t u(\mathbf{r},t) = D_u \Delta u + \kappa_2\, u - u^3 - \kappa_3 v - \kappa_4 w + \kappa_1, \tag{1a}$$

$$\tau \partial_t v(\mathbf{r},t) = D_v \Delta v + u - v, \tag{1b}$$

$$\theta \partial_t w(\mathbf{r},t) = D_w \Delta w + u - w, \quad \mathbf{r} \in \Omega, \tag{1c}$$

where $\Delta = \partial_x^2 + \partial_y^2$ represents the Laplacian in Cartesian coordinates, $\mathbf{r}$ is the position vector in the domain Ω, $\mathbf{r} = (x,y)^T \in \Omega \subset \mathbb{R}^2$, and time t. While the activator u activates the production of v and w and at least near $u = 0$ for itself, the components v and w act as inhibitors for positive kinetic parameters κ_3 and κ_4. The molecular diffusion coefficients D_u, D_v, and D_w are positive, dimensionless constants and τ and θ set the time scales of the temporal evolution of v and w, respectively.

For $\kappa_4 = 0$, (1c) decouples from the other two equations and (1a)-(1b) reduce to the FitzHugh-Nagumo model [61, 62]. While the FitzHugh-Nagumo model does not exhibit stable localized structures in two and three spatial dimensions [63], these can be stabilized by a global feedback term [64]. However, multiple moving spot solutions cannot be obtained in a two-component system with global feedback as the latter does not take account of antisymmetric disturbances [65]. One way to overcome this difficulty is to introduce a fast, $\theta \ll \tau$, and strongly diffusive, $D_w \gg D_u$, second inhibiting component which plays the role of a negative local feedback. Moreover, a nonvanishing kinetic parameter κ_1 violates the inversion symmetry $(u,v,w) \to (-u,-v,-w)$ and results in the existence [66] and stability [67, 68] of localized solutions to (1). Beside stationary or traveling localized patterns, in what follows shortly coined spots, (1) exhibits a variety of patterns as e.g. peanut patterns [69], breathing solitons [70], and jumping oscillons [71].

The system (1) was first introduced by Purwins and co-workers in [59] as a phenomenological model for a planar dc gas-discharge system with a high-ohmic semiconductor electrode. The activator u and inhibitor v were interpreted as the current density and voltage drop over the high-ohmic electrode, respectively. The second inhibitor w can be related to the surface charge or other characteristics of the high-ohmic layer [50] and the additive bifurcation parameter κ_1 is associated with the applied voltage [72]. From a nonlinear dynamics point of view, we consider (1) as a simple generic model system for the investigation of localized patterns in RD systems. Three-component models have attracted much attention in recent years to describe various chemical, biological, and physical systems like the photosensitive BZ reaction [11], the BZ-AOT reaction [73], CO oxidation on Pt(110) [74], blood clotting [75], and Dictyostelium amoebae [76], to name a few.

If the additive, constant parameter κ_1 in (1) is replaced by a spatially distributed function $\kappa_1(\mathbf{r})$, one can identify the latter either as an applied static control, e.g., light illumination through a mask [12], or as a inhomogeneity of the medium [77, 68].

The interaction of traveling spots with heterogeneities of jump type in 1D [78] and 2D [68, 69] have been intensively studied and penetration, rebound, annihilation, oscillation, and stationary as well as oscillatory pinning are observed. In figure S1 in the supplemental information, we depict the spot's response to a circular defect of jump type in the additive parameter κ_1, i.e., the value of κ_1 changes discontinuously from the background value κ_1^{back} to κ_1^{het} inside the heterogeneity. Besides the above mentioned outcomes, we find alternative scenarios of spot-defect-interactions like continuous creation of spots inside the heterogeneity as well as stable circular motion both inside and outside at the defect's edge. Especially, if any system component is associated with the temperature in an exothermic chemical reaction, pinning of temperature hot zones (*hot spots*) [79] to local heterogeneities in the medium and collisions with reactor boundaries must be prevented for safety reasons. For this purpose, we develop an efficient open-loop control scheme allowing us to guide and orientate localized patterns along a pre-given trajectory inside a two-dimensional spatial domain. We sketch our idea on analytical control and recall optimal control of RD patterns in the following section.

2. Position control of spot solutions

2.1. Analytical position control

We consider a controlled RD system of the general form

$$\partial_t \mathbf{U}(\mathbf{r},t) - \mathbb{D}\Delta\mathbf{U}(\mathbf{r},t) - \mathbf{R}(\mathbf{U}(\mathbf{r},t)) = \mathbb{B}\mathbf{f}(\mathbf{r},t). \tag{2a}$$

Here, $\mathbf{U}(\mathbf{r},t) = (u_1(\mathbf{r},t),\dots,u_n(\mathbf{r},t))^T$ is a vector of n state components in the two-dimensional spatial domain $\Omega \subset \mathbb{R}^2$ with $\mathbf{r} = (x,y)^T$. Assuming an isotropic medium, the $n \times n$ matrix of diffusion coefficients $\mathbb{D}$ is a diagonal matrix of the form $\mathbb{D} = \operatorname{diag}(D_1,\dots,D_n)$. The reaction kinetics are encoded in the vector $\mathbf{R}(\mathbf{U}) = (R_1(\mathbf{U}),\dots,R_n(\mathbf{U}))^T$ which, in general, is a nonlinear function of the state. For the exemplarily chosen RDS (1), the quantities $\mathbf{U}$, $\mathbb{D}$, and $\mathbf{R}$ are identified by $\mathbf{U} = (u,v,w)^T$, $\mathbb{D} = \operatorname{diag}(D_u, D_v/\tau, D_w/\theta)$, and $\mathbf{R} = \big(\kappa_2\, u - u^3 - \kappa_3 v - \kappa_4 w + \kappa_1, (u-v)/\tau, (u-w)/\theta\big)^T$, respectively.

Equation (2a) must be supplemented with an initial condition

$$\mathbf{U}(\mathbf{r},t_0) = \mathbf{U}_0(\mathbf{r}), \tag{2b}$$

and appropriate boundary conditions. Here, we consider a rectangular domain Ω given by $x_a \le x \le x_b$ and $y_a \le y \le y_b$ with periodic boundary conditions such that $\mathbf{U}$ as well as its first derivatives in the direction normal to the boundary are periodic,

$$\begin{aligned} \mathbf{U}(x_a,y,t) &= \mathbf{U}(x_b,y,t), & \frac{\partial}{\partial x}\mathbf{U}(x_a,y,t) &= \frac{\partial}{\partial x}\mathbf{U}(x_b,y,t), \\ \mathbf{U}(x,y_a,t) &= \mathbf{U}(x,y_b,t), & \frac{\partial}{\partial y}\mathbf{U}(x,y_a,t) &= \frac{\partial}{\partial y}\mathbf{U}(x,y_b,t). \end{aligned} \tag{2c}$$

The quantity $\mathbf{f}(\mathbf{r},t) = (f_1(\mathbf{r},t),\dots,f_m(\mathbf{r},t))^T$ with $m \in \mathbb{N}$ on the right hand side of (2a) represents the vector of spatially distributed control signals. We presume that the control acts everywhere within the spatial domain Ω and at all times t. The $n \times m$ matrix $\mathbb{B}$ determines which state components are directly affected by the control signals. A system with strictly less independent control signals than state components,

$m < n$, is called an *underactuated* system. Contrary, it is called a *fully actuated* system if $m = n$ and $\mathbb{B}$ is a regular square matrix, i.e., the inverse of $\mathbb{B}$ also exists. In what follows, we focus on fully actuated systems and set $\mathbb{B}$ equal to the identity matrix $\mathbb{1}$. A detailed discussion for underactuated systems can be found in [80] and, in particular, we study the limiting case of singular control, i.e., $\mathbb{B}\mathbf{f}(\mathbf{r},t) \propto (f_1(\mathbf{r},t), 0, \ldots, 0)^T$, in section 3.4.

The goal of our control $\mathbf{f}$ is to enforce a state $\mathbf{U}$ which follows a given *desired distribution* $\mathbf{U}_d(\mathbf{r},t) = (u_{1,d}(\mathbf{r},t), \ldots, u_{n,d}(\mathbf{r},t))^T$ as closely as possible everywhere in the domain Ω and for all times $0 \leq t \leq T$. We call a desired distribution $\mathbf{U}_d$ *exactly realizable* if there exists a control $\mathbf{f}$ such that the controlled state $\mathbf{U}$ equals $\mathbf{U}_d$ everywhere in Ω and for all times, i.e., $\mathbf{U}(\mathbf{r},t) = \mathbf{U}_d(\mathbf{r},t)$. For fully actuated systems, a simple analytical result for the control can be obtained with the help of the following observation. Usually, (2a) is viewed as a partial differential equation (PDE) for the states $\mathbf{U}$ with control signals $\mathbf{f}(\mathbf{r},t)$ acting as spatio-temporal perturbations, and the response of a given pattern in the presence of $\mathbf{f}$ is studied [81]. Here, we view (2a) as a conditional equation for the control $\mathbf{f}$. Inserting simply $\mathbf{U}_d$ for $\mathbf{U}$ in (2a) and solving for $\mathbf{f}$ yields

$$\mathbf{f}_{\text{ins}}(\mathbf{r},t) = \mathbb{B}^{-1}\{\partial_t \mathbf{U}_d(\mathbf{r},t) - \mathbb{D}\Delta\mathbf{U}_d(\mathbf{r},t) - \mathbf{R}(\mathbf{U}_d(\mathbf{r},t))\}. \tag{3}$$

For $\mathbf{U}_d$ to be exactly realizable, two more conditions must be satisfied: First, the initial condition for the controlled state, (2b), must coincide with the initial state of the desired distribution, $\mathbf{U}(\mathbf{r},0) = \mathbf{U}_d(\mathbf{r},0)$. Second, all boundary conditions for the desired distribution $\mathbf{U}_d$ have to comply with the boundary conditions for $\mathbf{U}$, (2c).

By using (3) in (2a) for the controlled RDS, it is easy to check that the proposed control indeed enforces the desired state $\mathbf{U}(\mathbf{r},t) = \mathbf{U}_d(\mathbf{r},t)$. Note that the control signal is well defined as long as the desired distribution is sufficiently smooth in the space-time cylinder $Q = \Omega \times [0,T]$ such that the evaluation of the derivatives $\partial_t \mathbf{U}_d$ and $\Delta\mathbf{U}_d$ yields continuous expressions. We emphasize the generality of the result (3): Apart from the boundary and initial conditions as well as mild requirements on the smoothness of the desired distributions $\mathbf{U}_d$, (3) gives a simple expression for the control signal for arbitrary $\mathbf{U}_d$. In the following, we refer to the control solution (3) as *insert control*.

This work's objective is to adapted the general control solution (3) to spot solutions of two-dimensional RDS. Spots are localized solutions to the uncontrolled RD system (2) with $\mathbf{f} = \mathbf{0}$. They propagate smoothly with a stationary wave profile $\mathbf{U}_c$ and velocity $\mathbf{v}_0$ such that, in a frame of reference $\boldsymbol{\xi} = (\xi_x, \xi_y)^T \equiv \mathbf{r} - \mathbf{v}_0 t$ co-moving with velocity $\mathbf{v}_0 = (v_0^x, v_0^y)^T$, $\mathbf{U}_c$ satisfies

$$\mathbf{0} = \mathbb{D}\Delta_{\boldsymbol{\xi}}\mathbf{U}_c(\boldsymbol{\xi}) + \mathbf{v}_0 \cdot \nabla_{\boldsymbol{\xi}}\mathbf{U}_c(\boldsymbol{\xi}) + \mathbf{R}(\mathbf{U}_c(\boldsymbol{\xi})). \tag{4}$$

Here, $\nabla_{\boldsymbol{\xi}} = (\partial_{\xi_x}, \partial_{\xi_y})^T$ and $\Delta_{\boldsymbol{\xi}} = \partial^2_{\xi_x} + \partial^2_{\xi_y}$ denote the component-wise gradient and Laplacian, respectively. We emphasize that stationary spots are also considered as spot solutions moving with zero velocity, $\mathbf{v}_0 = \mathbf{0}$. While traveling spots with $\mathbf{v}_0 \neq \mathbf{0}$ usually exhibit an asymmetry parallel to the propagation direction, see figure 1(a), stationary spots are often rotationally symmetric and do not exhibit a certain orientation.
In general, a spot is characterized by its wave profile $\mathbf{U}_c$ and three parameters, namely its position in x- and y- direction as well as its orientation, in the two-dimensional plane. Thereby, we refer to the maximum value of a chosen component, as e.g. the

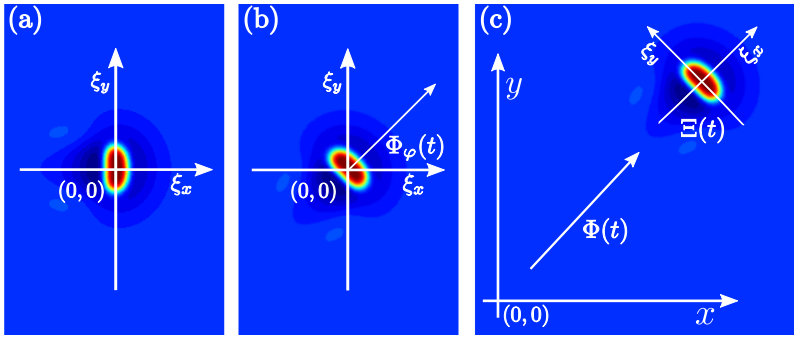

Figure 1. Construction of the desired distribution $\mathbf{U}_d(\mathbf{r},t)$ defined by (5). (a) Wave profile of the unperturbed activator distribution in the spot model (1), $u_c(\boldsymbol{\xi})$, being centered in the co-moving and co-rotating frame of reference at $\boldsymbol{\xi}=(0,0)^T$. First, (b) counter-clockwise rotation of $u_c(\boldsymbol{\xi})$ according to the desired orientation $\Phi_\varphi(t)$ and then (c) shifting of the received solution in virtue of the translation protocols of motion $\boldsymbol{\Phi}(t)=(\Phi_x(t),\Phi_y(t))^T$.

activator u in model (1), as the current position of traveling spots as well as to the point of symmetry for stationary spots.

Next, we propose that the applied control $\mathbf{f}(\mathbf{r},t)$ moves the spot solution according to a prescribed protocol of motion (POM) $\boldsymbol{\Xi}(t)=(\boldsymbol{\Phi}(t),\Phi_\varphi(t))^T$ with position vector $\boldsymbol{\Phi}(t)=(\Phi_x(t),\Phi_y(t))^T$ and rotation $\Phi_\varphi(t)$. A desired distribution following a prescribed protocol of motion while simultaneously preserving the uncontrolled wave profile $\mathbf{U}_c$ is constructed as

$$\mathbf{U}_d(\mathbf{r},t)=\mathbf{U}_c(\mathbb{A}(-\Phi_\varphi(t))\,(\mathbf{r}-\boldsymbol{\Phi}(t))), \tag{5}$$

where $\mathbb{A}(\alpha)=[\cos(\alpha)\,,-\sin(\alpha);\sin(\alpha)\,,\cos(\alpha)]$ equals the clockwise rotation matrix in 2D. For the desired distribution (5) to be exactly realizable, the initial condition of the system must be a spot solution of the form $\mathbf{U}(\mathbf{r},t_0)=\mathbf{U}_c(\mathbb{A}(-\phi_0)\,(\mathbf{r}-\mathbf{r}_0))$, which yields for the initial values of the POM $\boldsymbol{\Phi}(t_0)=\mathbf{r}_0$ and $\Phi_\varphi(t_0)=\phi_0$, respectively. Inserting the desired distribution (5) into the general control solution (3) leads to

$$\mathbf{f}(\mathbf{r},t)=\left[-\left(\mathbb{A}_z(-\Phi_\varphi(t))\,\dot{\boldsymbol{\Xi}}(t)\right)\cdot\tilde{\nabla}_{\boldsymbol{\xi}}\mathbf{U}_c(\boldsymbol{\xi})-\mathbb{D}\Delta_{\boldsymbol{\xi}}\mathbf{U}_c(\boldsymbol{\xi})-\mathbf{R}(\mathbf{U}_c(\boldsymbol{\xi}))\right]_{\boldsymbol{\xi}=\boldsymbol{\xi}(t)}, \tag{6}$$

with $\boldsymbol{\xi}(t)=\mathbb{A}(-\Phi_\varphi(t))\,(\mathbf{r}-\boldsymbol{\Phi}(t))$. For the sake of a compact notation, we introduced the differential operator $\tilde{\nabla}_{\boldsymbol{\xi}}=(\partial_{\xi_x},\partial_{\xi_y},\partial_\varphi)^T$ with the angular derivative $\partial_\varphi=-\xi_y\partial_{\xi_x}+\xi_x\partial_{\xi_y}$, the dot represents the derivative with respect to time t, and $\mathbb{A}_z(\alpha)$ denotes the clockwise rotation matrix around the z-axes in 3D, $\mathbb{A}_z(\alpha)=\mathrm{diag}(\mathbb{A}(\alpha),1)$. Finally, we obtain the *analytical control* signal $\mathbf{f}_{\mathrm{ana}}$ for position control

$$\mathbf{f}_{\mathrm{ana}}(\mathbf{r},t)=\left[\left(\begin{pmatrix}v_0^x\\v_0^y\\0\end{pmatrix}-\mathbb{A}_z\left(-\Phi_\varphi(t)\right)\begin{pmatrix}\dot{\Phi}_x(t)\\\dot{\Phi}_y(t)\\\dot{\Phi}_\varphi(t)\end{pmatrix}\right)\cdot\tilde{\nabla}_{\boldsymbol{\xi}}\right]\mathbf{U}_c(\boldsymbol{\xi})\Big|_{\boldsymbol{\xi}=\boldsymbol{\xi}(t)}, \tag{7}$$

by using relation (4) for the spot profile .

The analytical solution (7) is composed of a sum of the Goldstone modes with time-dependent prefactors $\mathbf{f}_{\mathrm{ana}}(\mathbf{r},t)=P_1(t)\partial_{\xi_x}\mathbf{U}_c(\boldsymbol{\xi})+P_2(t)\partial_{\xi_y}\mathbf{U}_c(\boldsymbol{\xi})+P_3(t)\partial_\varphi\mathbf{U}_c(\boldsymbol{\xi})$. The Goldstone modes are the right eigenvectors to the linear stability operator of (4)

to the eigenvalue zero and they are associated to the translational and rotational invariance of the traveling wave solution $\mathbf{U}_c$ in $\mathbb{R}^2$. If the prescribed POM $\boldsymbol{\Xi}(t)$ coincides with the spot's natural motion, then all pre-factors vanish identically and, as expected, $\mathbf{f}_{\text{ana}}$ vanishes everywhere in Q. Suppose the natural direction of motion coincides with the ξ_x-axis, i.e., $v_0^y = 0$, and one controls solely the spot's position in ξ_x, i.e., $\Phi_y(t) = \Phi_\varphi(t) = 0$, then P_2 and P_3 vanish and (7) simplifies to $\mathbf{f}_{\text{ana}}(\mathbf{r}, t) = (v_0^x - \dot{\Phi}_x(t))\partial_{\xi_x}\mathbf{U}_c(\boldsymbol{\xi})|_{\boldsymbol{\xi}=(\mathbf{r}-\boldsymbol{\Phi}_{(t)})}$. Obviously, the magnitude of the applied control signal is determined by the difference between the intrinsic velocity v_0^x and the current prescribed spot's velocity $\dot{\Phi}_x(t)$. Because the spot's profile is localized in the sense that its spatial derivatives decay to zero, $\lim_{\|\boldsymbol{\xi}\|\to\infty} \partial_{\boldsymbol{\xi}}\mathbf{U}_c = 0$, the control signal is localized at the presumed spot's position $\Phi_x(t)$ and vanishes everywhere else.

Remarkably, any reference to the reaction functions $\mathbf{R}$ drops out from the expression for the analytical control (7). This is of great advantage for applications without or only incomplete knowledge of the underlying reaction kinetics $\mathbf{R}$. Furthermore, the control signals can be pre-computed for the complete time interval $[0, T]$ once the propagation velocity $\mathbf{v}_0$ and the uncontrolled wave profile $\mathbf{U}_c$ have been measured with sufficient accuracy. Consequently, a continuous recording of the system is not necessary in contrast to closed-loop or feedback control loops. We stress that the approach to position control presented above is not limited to traveling or stationary spot solutions in RD systems. It can easily be extended to other solutions of RDS as e.g. rigidly rotating patterns like spiral waves in two and scroll waves in three-dimensional RDS. Furthermore, the approach is not at all restricted to evolution equations of RDS type but also applies to e.g. neural field equations governed by integro PDEs which exhibit localized bump solutions similar to spots in RDS [82, 83].

Despite the advantages of our analytical solution stated above, there are limits for it as well. While for the analytic approach (7) no bounds for the control signal are born in mind, in applications it is often necessary to impose inequality constraints in form of upper and lower bounds on the control. For example, the intensity of a heat or light source deployed as control is bounded by technical reasons. Because $\mathbf{f}_{\text{ana}}$ is proportional to the slope of the controlled wave profile $\mathbf{U}_c'$, the magnitude of the applied control may locally attain non-realizable values. In addition, we presume that the complete spatial domain Ω is accessible by the control signal. Often, this assumption is not realizable in experiments, where the application of $\mathbf{f}$ is often restricted to subsets of Ω. However, notable exceptions, as e.g. the already mentioned photosensitive BZ reaction [11], optogenetic control of cells [84], optical bistable systems [32], and CO oxidation on Pt surfaces [28], exist. Furthermore, $\mathbf{f}_{\text{ana}}$ cannot be applied to desired trajectories $\mathbf{U}_d$ which do not comply with initial as well as boundary conditions or which are non-smooth. Most important, the restriction to fully actuated systems is overly restrictive in applications. The number of state components is usually larger than the amount of control signals, and introducing additional means of spatio-temporal control to increase the number of independent control signals is often not feasible. Although the analytic approach can be extended to underactuated systems by entailing additional assumptions about the desired distribution, this usually leads to control signals which strongly deform the wave profile $\mathbf{U}_c$ for some state components, see section 3.4. While all these cases cannot be treated within the analytical approach proposed here, optimal control can deal with many of these complications.

2.2. Optimal control

In addition to the previously derived insert (3) and analytical control (7), we employ an optimal control strategy that aims to determine a control $\mathbf{f}$ such that the state $\mathbf{U}$ coincides with the desired spatio-temporal distribution $\mathbf{U}_d$ as well. Contrary to insert and analytical control, an *optimal* control $\mathbf{f}_{\text{opt}}$ does not enforce exclusively $\mathbf{U}$ to follow $\mathbf{U}_d$ in Q; it rather minimizes a so-called objective functional J. Thus, we simply define J as a non-negative tracking-type functional

$$J(\mathbf{U},\mathbf{f}) = \frac{1}{2}\sum_{i=1}^{n}\left[\int_0^T\!\!\int_\Omega \left(u_i - u_{i,d}\right)^2 \mathrm{d}\mathbf{r}\,\mathrm{d}t \;+\nu \int_0^T\!\!\int_\Omega f_i^2 \mathrm{d}\mathbf{r}\,\mathrm{d}t\right], \tag{8}$$

where $\mathbf{U}$ satisfies the controlled state equation associated to $\mathbf{f}$ with respect to given associated initial and boundary condition, cf. equations (2). The first term appearing in J measures the distance between the actual solution $\mathbf{U}$ and the desired trajectory $\mathbf{U}_d$ up to the terminal time T in an $L^2(Q)$-sense, i.e., $\|\mathbf{h}\|^2_{L^2(Q)} = \int_0^T\!\int_\Omega \mathbf{h}^2 \mathrm{d}\mathbf{r}\mathrm{d}t$. Usually, one cannot guarantee to find a control $\mathbf{f}$ that enforces the state $\mathbf{U}$ to equal the desired trajectory $\mathbf{U}_d$ everywhere in time and space. In order to ensure that the problem is mathematically well-defined and the objective functional has a minimum rather than only an infimum, one can add a so-called Tikhonov-regularization term to the non-negative objective functional J; being represented by the second term in (8). In fact, the small but finite positive value of the regularization parameter ν guarantees the existence of an optimal control $\mathbf{f}_{\text{opt}}$ that minimizes the objective functional J (8) for $\Omega \subset \mathbb{R}^q, q = 1, 2, 3$, [85] and the squared $L^2(Q)$-norm of $\mathbf{f}$ might be interpreted as a cost to achieve a certain state $\mathbf{U}$. Alternatively, one can introduce additional constraints such as upper and lower limits for the amplitude of the control signal [20].

For exactly realizable desired distributions $\mathbf{U}_d$ the distance between the actual solution $\mathbf{U}$ and $\mathbf{U}_d$ vanishes. If additionally $\nu = 0$, then J attains its minimally possible value $J = 0$. Consequently, the analytical control solution (3) for exactly realizable desired distributions is the solution to an unregularized optimal control problem, cf. [46, 80].

If $\mathbf{U}_d$ is not exactly realizable, the controlled state $\mathbf{U}$ must be obtained as part of the solution to the optimal control problem. The minimization of J must be performed with respect to state $\mathbf{U}$ and control $\mathbf{f}$. Expressing $\mathbf{U}$ in terms of $\mathbf{S}(\mathbf{f})$, where $\mathbf{S} : \mathbf{f} \mapsto \mathbf{U}$ is the solution operator to (2) in Q, justifies the definition of a reduces objective functional $J(\mathbf{f}) := J(\mathbf{S}(\mathbf{f}), \mathbf{f})$. In order to minimize $J(\mathbf{f})$, its first derivative with respect to $\mathbf{f}$ has to equal zero; yielding the necessary optimality conditions

$$\left[\int_0^T\!\!\int_\Omega \left(\mathbf{S}'(\mathbf{f}_{\text{opt}})\right)_i \left(\left(\mathbf{S}(\mathbf{f}_{\text{opt}})\right)_i - u_{i,d}\right) \mathrm{d}\mathbf{r}\,\mathrm{d}t \;+\nu \int_0^T\!\!\int_\Omega f_{i,_{\text{opt}}} \mathrm{d}\mathbf{r}\,\mathrm{d}t\right] = 0, \quad \forall i = 1,\ldots,n. \tag{9}$$

Thereby, the state is constrained to satisfy the controlled state equation together with given initial and boundary conditions, cf. equations (2). Similar as in ordinary minimization problems, a constrained minimization can be transformed to an unconstrained minimization problem by introducing Lagrange multipliers $\mathbf{P}(\mathbf{r},t) = (p_1(\mathbf{r},t),\ldots,p_n(\mathbf{r},t))^T$, also called the *adjoint state*. By means of the latter, (9) can

be reformulated

$$\int_0^T \iint_\Omega \left(\mathbf{S}'(\mathbf{f}_{\rm opt})\right)_i \left(\left(\mathbf{S}(\mathbf{f}_{\rm opt})\right)_i - u_{i,d}\right) \mathrm{d}\mathbf{r}\,\mathrm{d}t = \int_0^T \iint_\Omega p_i \mathrm{d}\mathbf{r}\,\mathrm{d}t\,, \quad \forall i = 1,\ldots,n, \tag{10}$$

whereby the adjoint state is the solution of the *adjoint equation*

$$-\partial_t \mathbf{P}(\mathbf{r},t) - \mathbb{D}\Delta\mathbf{P}(\mathbf{r},t) - \mathbf{J}_{\mathbf{R}}^T(\mathbf{U}(\mathbf{r},t))\mathbf{P}(\mathbf{r},t) = \mathbf{U} - \mathbf{U}_d \quad \text{in} \quad Q, \tag{11}$$

subject to terminal condition $\mathbf{P}(\cdot,T) = \mathbf{0}$ in Ω and periodic boundary conditions in $\partial\Omega$. Here, $\mathbf{J}_{\mathbf{R}}^T$ denotes the transposed Jacobian matrix of $\mathbf{R}$ with respect to $\mathbf{U}$.

Due to the mixed initial and terminal conditions for $\mathbf{U}$ and $\mathbf{P}$ its is rarely possible find numerical solutions to optimal control by a direct integration method. Here we use an iterative algorithm of gradient type which proceeds as follows: For $k = 1$ and an initial guess $\mathbf{f}_0$ for the control, we compute the state $\mathbf{U}_k$ as the solution to (2) as well as the adjoint state $\mathbf{P}_k$ as the solution to (11). The gradient $\mathbf{d}_k$ of J with respect to $\mathbf{f}$ is calculated as $\mathbf{d}_k = \mathbf{P}_k + \nu\mathbf{f}_{k-1}$ and defines a direction of descent in function space. A new control $\mathbf{f}_k$ is iteratively obtained by

$$\mathbf{f}_k := \mathbf{f}_{k-1} + s\,\mathbf{d}_k, \tag{12}$$

where s denotes a suitable step size [20, 21]. If the new control $\mathbf{f}_k$ satisfies an appropriate termination condition for the optimization, then the algorithm stops and the final solution $\mathbf{f}_k$ is identified with the optimal control signal $\mathbf{f}_{\rm opt}$. If this is not the case, the steps above need to be repeated iteratively for $k := k + 1$. The termination condition applied here is that the gradient $\mathbf{d}_k$ of J with respect to $\mathbf{f}$ is vanishing within numerical accuracy, i.e., $\|\mathbf{d}_k\| \leq \varepsilon$ for sufficiently small $\varepsilon > 0$. The convergence of a gradient-type method can be fairly slow and thus a maximum iteration number should be defined. Many modifications of the basic algorithm sketched above exist and often lead to a better performance, as e.g. the conjugate gradient method [42]. However, all iterative algorithms require multiple solutions of state and adjoint state equation, resulting in a rapidly increasing computational cost of numerical optimal control with the number of spatial dimensions and the length of the time interval.

On the other hand, the scope of optimal control can be extended in many ways, and much more general objective functionals as stated above can be covered. We mention sparse optimal control [20], which yields effective controls acting only in the most sensitive spatial or temporal regions of a controlled solution while it vanishes elsewhere. Moreover, optimal control can easily deal with restrictions of control signals to prescribed spatial regions as well as restrictions of the amplitude of state or control in the form of inequalities, i.e., $-\infty < f_a \leq f_i(\mathbf{r},t) \leq f_b < \infty$, $\forall i = 1,\ldots,n$. Technical details as well as examples can be found in [20, 46].

3. Numerical examples

Below, we apply the analytical (7) and optimal control (10) on traveling spot solutions to the three component RDS (1). Both the controlled RD system (2a) and the adjoint equation (11) are solved on a squared domain $\Omega = (-0.5, 0.5] \times (-0.5, 0.5]$ with periodic boundary conditions (2c) both in x and y. A regular discretization of the domain by 256 grid points in each direction with spatial step sizes of $dx = dy = 1/256$

	D_u	D_v	D_w	τ	κ_1	v_0^x
set 1	$1.0 \cdot 10^{-4}$	$1.86 \cdot 10^{-4}$	$9.6 \cdot 10^{-3}$	48.0	-6.92	$2.599 \cdot 10^{-3}$
set 2 [68]	$0.9 \cdot 10^{-4}$	$1.00 \cdot 10^{-3}$	$1.0 \cdot 10^{-2}$	40.0	-7.30	$1.776 \cdot 10^{-3}$

Table 1. Parameter sets used in the numerical simulations. The remaining system kinetic coefficients equal in both sets and are kept fixed at $\theta = 1$, $\kappa_2 = 2$, $\kappa_3 = 1$, and $\kappa_4 = 8.5$.

is employed and the Laplacian Δ is approximated by a 5-point stencil. We emphasize that the spatial domain has to be chosen sufficiently large in order to avoid self-interaction of the spot solutions in the periodic simulation domain. Due to the significant computational cost of the optimal control algorithm we choose a moderate temporal resolution of $dt = 0.1$. For maximal stability the time evolution is computed with an implicit Euler method. We limit the maximum number of iterations for the numerical optimal control to $N_{\text{iter}} = 50$ and set the terminal condition to $\|\mathbf{d}_k\| < 10^{-8}$ in our gradient-type method to calculate $\mathbf{f}_{\text{opt}}$. If not stated otherwise, we keep the Tikhonov-regularization parameter fixed at $\nu = 10^{-7}$.

Numerical simulations are initialized with an uncontrolled stable spot profile $\mathbf{U}_c(\mathbf{r}, t)$ obtained from a sufficiently long simulation such that any transient modes have decayed and the natural spot velocity $\mathbf{v}_0$ can be measured with adequate accuracy. Without loss of generality, we set the spot's natural direction of motion to coincide with the x-axis, i.e., $v_0^y = 0$. If not stated otherwise, the parameter set 1 in table 1 is used for the kinetic model parameters.

The desired distribution $\mathbf{U}_d(\mathbf{r}, t)$ (5) for position control involves the shifted and rotated spot profile and it is computed with spectral methods. In a first step, the uncontrolled spot profile $\mathbf{U}_c(\mathbf{r}, t)$ is rotated around $(0, 0)^T$ in the spatial domain by an angle given by the rotational POM $\Phi_\varphi(t)$, see figure 1(b). In a second step, the shift as given by the translational POM $\mathbf{\Phi}(t) = (\Phi_x(t), \Phi_y(t))^T$, cf. figure 1(c), is computed in Fourier space by multiplying the Fourier transform $\mathcal{F}\{\cdot\}$ of the previously rotated spot by the factor $\exp(-i\mathbf{k} \cdot \mathbf{\Phi}(t))$ with wave vector $\mathbf{k} = (k_x, k_y)^T$, followed by the inverse Fourier transform $\mathcal{F}^{-1}\{\cdot\}$. The spatio-temporal evolution of the analytic control signals (7), can be computed in an analogous manner. First, the derivatives in x and in y are obtained numerically in Fourier space using $\partial_x \mathbf{U}_c = \mathcal{F}^{-1}\{ik_x \mathcal{F}\{\mathbf{U}_c\}\}$ and $\partial_y \mathbf{U}_c = \mathcal{F}^{-1}\{ik_y \mathcal{F}\{\mathbf{U}_c\}\}$, respectively. The angular derivative is given as the linear combination $\partial_\varphi \mathbf{U}_c = -y\partial_x \mathbf{U}_c + x\partial_y \mathbf{U}_c$. Second, all derivatives are rotated according to the orientational POM $\Phi_\varphi(t)$, followed by a shift computed in Fourier space as given by $\mathbf{\Phi}(t)$.

3.1. Position control

In our first example, we aim to shift the spot's position along a Lissajous curve without controlling its orientation. Hence, the chosen protocol of motion $\mathbf{\Xi}(t) = (\Phi_x(t), \Phi_y(t), \Phi_\varphi(t))^T$ is given by

$$\Phi_x(t) = r\,\sin(4\pi\, t/T)), \quad \Phi_y(t) = r\,\sin(6\pi\, t/T)), \quad \text{and} \quad \Phi_\varphi(t) = 0, \tag{13}$$

with radius $r = 0.2$ and protocol duration $T = 200$. Figure 2(a) depicts the time evolution of the activator distribution $u(\mathbf{r}, t)$ under the action of the analytic control $\mathbf{f}_{\text{ana}}(\mathbf{r}, t)$ shown in figure 2(b). In both plots, the prescribed Lissajous trajectory (13) is indicated by the dashed line. One notices that the spot follows

the trajectory as desired and its orientation is not influenced by the control, i.e., the symmetry axis coincides with the x-axis at any time. In contrast to that, the control signal changes its orientation at any instant of time. Indeed, in the absence of orientation control the analytic control signal (7) can be expressed by the gradient of $\mathbf{U}_c$ projected onto the tangential vector $\mathbf{T}(t)$ on the Lissajous curve, $\mathbf{f}_{\text{ana}}(\mathbf{r},t) = \left[\left(v_x^0 - \dot{\Phi}_x(t)\right)\partial_{\xi_x}\mathbf{U}_c\left(\boldsymbol{\xi}(t)\right) - \dot{\Phi}_y(t)\partial_{\xi_y}\mathbf{U}_c\left(\boldsymbol{\xi}(t)\right)\right]_{\boldsymbol{\xi}(t)=\mathbf{r}-\boldsymbol{\Phi}(t)} \simeq \mathbf{T}(t)\cdot\nabla\,\mathbf{U}_c$. Furthermore, the control is localized at the presumed spot's position $\boldsymbol{\Phi}(t)$ and vanishes far away from it. Noteworthy, the magnitude of the activator's control signal is of the same order as the local reaction terms (1) despite that the average speed $\bar{v} = L_{\text{curve}}/T \approx 6v_x^0$ along the studied Lissajous curve (13) with arc length L_{curve} is almost six times larger than the spot's intrinsic speed. The control signals applied to the inhibitors v and w are one and two magnitudes smaller than the activator's control, respectively. In the following, we focus solely on the activator's control and omit a detailed discussion of the controls f_v and f_w.

The video [SI_video1] in the supplemental information shows the dynamics of all state components $\mathbf{U}$ as well as the analytical and optimal controls. On that scale there is no distinguishable difference between the two control signals. Both are localized at the spot's position and their magnitudes change proportional to $|\dot{\boldsymbol{\Phi}}(t)|$. For a quantitative comparison, we compute the relative errors between insert, analytical, and optimal control signals measured by the $L^1(\Omega)$-norm

$$\|h(t)\|_{L^1(\Omega)} = \int_\Omega |h\left(\mathbf{r},t\right)|\mathrm{d}\mathbf{r}\,. \tag{14}$$

Here, $|h\left(\mathbf{r},t\right)|$ indicates the absolute value of h at position $\mathbf{r}$ and time t. Since the POM starts to repeat after $T/2$, $\Phi_y(t+T/2) = -\Phi_y(t)$, we show only the normalized error for the first half of the protocol in figure 2(c).

It turns out that the relative error between our analytic $f_{u,\text{ana}}$ and the optimal control $f_{u,\text{opt}}$ (dash-dotted line) is satisfactory and ranges from 2% to 8%. While the numerical evaluation of $\mathbf{f}_{\text{ana}}$ is limited by the accuracy of the first spatial derivatives $\tilde{\nabla}_{\boldsymbol{\xi}}\mathbf{U}_c$, the numerical computations of $\mathbf{f}_{\text{opt}}$ is affected by errors arising both in the discretization of space and time. We stress that $\mathbf{f}_{\text{ana}}$ is computed by using spectral differentiation, while we have to use finite difference stencils for the simulation of both the state (2) and the adjoint equation (11) in order to reduce computational costs. Nevertheless, the limiting error arises from the time step being chosen in the implicit Euler-scheme. Despite that the latter is A-stable, the local truncation error is $\mathcal{O}(dt^2)$ and the error at a specific time t is of the order of $\mathcal{O}(dt)$. Consequently, one observes that the relative error $\|f_{u,\text{ana}}(t) - f_{u,\text{opt}}(t)\|_{L^1(\Omega)}$ is bounded from above by $dt = 0.1$. On the other hand, one notices that the relative error between the insert $f_{u,\text{ins}}$ and the optimal control $f_{u,\text{opt}}$ (solid line) fluctuates around 10^{-4} for all times. Both controls are computed by using the identical finite differences scheme in space and are based on the same pre-defined desired distribution $\mathbf{U}_d$. Moreover, the time derivative $\partial_t\mathbf{U}_d$ in (3) is computed by a forward difference for which the error at a given time is also of the order of $\mathcal{O}(dt)$. Consequently, roundoff errors do not amplify. Since $f_{u,\text{opt}}$ is almost identical to $f_{u,\text{ins}}$, the temporal behavior of $\|f_{u,\text{ana}}(t) - f_{u,\text{ins}}(t)\|_{L^1(\Omega)}$ (markers) leads to quite analogue results as $\|f_{u,\text{ana}}(t) - f_{u,\text{opt}}(t)\|_{L^1(\Omega)}$ (dash-dotted line). We emphasize that higher order schemes for ∂_t, like central differences with error $\mathcal{O}(dt^2)$, result in a smaller relative error between $f_{u,\text{ins}}$ and $f_{u,\text{ana}}$ but in a slightly larger one for $\|f_{u,\text{opt}}(t) - f_{u,\text{ins}}(t)\|_{L^1(\Omega)}$.

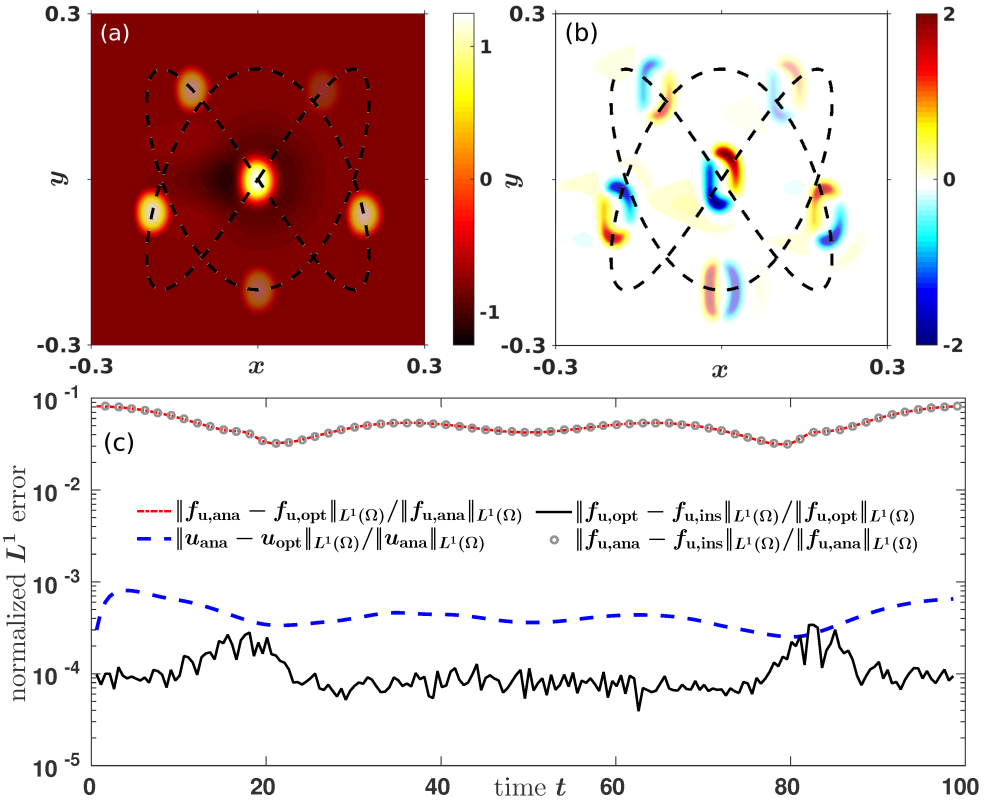

Figure 2. Position control along the Lissajous curve (13). (a) Time evolution of the activator distribution $u(\mathbf{r}, t)$ obtained from numerical simulation of (1)-(2a) with control $\mathbf{f}_{\mathrm{ana}}$ given by (7) at different instants of time $t = \{10, 50, 90, 130, 170, 200\}$. (b) Distribution of the activator component of $\mathbf{f}_{\mathrm{ana}}$ acting on the activator u, $f_{u,\mathrm{ana}}(\mathbf{r}, t)$, at the same instants of time. In both subfigures (a) and (b), the dark dashed line indicates the Lissajous curve and the decreasing transparency marks consecutive moments. (c) Temporal behavior of the relative $L^1(\Omega)$ error (14) between insert $f_{u,\mathrm{ins}}$, (3), analytical $f_{u,\mathrm{ana}}$, (7), and optimal activator control signals $f_{u,\mathrm{opt}}$, (8) during $t \in [0, T/2]$. The controlled spot dynamics (1) with system parameters given by set 1 in table 1 is simulated on a $(-0.5, 0.5] \times (-0.5, 0.5]$ domain with periodic boundary conditions and an implicit Euler method in time [SI_video1].

Finally, we display the relative error between the analytically controlled activator distribution and the one obtained by means of optimal control, $\|u_{\mathrm{ana}}(t) - u_{\mathrm{opt}}(t)\|_{L^1(\Omega)}/\|u_{\mathrm{ana}}(t)\|_{L^1(\Omega)}$ as the dashed line in figure 2(c). Despite that the relative error between the control signal is of the order 10^{-1}, the relative error between the activator states is less than 10^{-3} at any time t, i.e., both controlled states agree remarkably well. In addition, the relative errors between the desired distribution $\mathbf{U}_d$ and the state solutions $\mathbf{U}_{\mathrm{ana}}$ and $\mathbf{U}_{\mathrm{opt}}$ are less than 10^{-7} in both cases (not shown explicitly in figure 2). This confirms, within numerical accuracy, that the analytical control (7) is indeed the solution to an unregularized optimal control problem. The same conclusion was obtained in our previous study of position control of reaction-diffusion front solutions in one spatial dimension, see [46].

We remind the reader that both the state equation (2) and the adjoint equation (11) have to be solved multiple times for computing an optimal control. To reduce numerical costs, we employ the method of Model Predictive Control and divide our optimal control problem in subproblems with a 4 time-step small time-horizon [46]. Thereby, each subproblem is solved with a gradient-type method. This iterative algorithm relies on an initial guess for the control signal. The closer the initial guess is to the final solution, the fewer steps are necessary for most established optimization methods to converge on the final solution. For instance, it takes on average $\bar{n}_{\text{iter}} \simeq 23$ iterations per time step when starting every iteration with an initial zero control. Taking the obtained control of the previous subproblem as initial control for the following one reduces the average number of iterations to $\bar{n}_{\text{iter}} \simeq 14$. Even much better if one takes advantage of the similarity of $\mathbf{f}_{\text{ins}}$ and $\mathbf{f}_{\text{opt}}$. Initiating every optimization subproblem with the corresponding insert control $\mathbf{f}_{\text{ins}}(\mathbf{r}, t)$ leads to a substantial computational speedup; on average the iteration stops after the first step independently of the controlled component, $\bar{n}_{\text{iter}} \simeq 1$.

Nevertheless, the optimal control algorithm requires much more computational resources compared to our analytic control. For instance, the computation of optimal position control along the Lissajous curve (13) with a short period of $T = 200$, i.e., 2000 time iterations steps with $dt = 0.1$, takes roughly 50 hours by using 3 cores (Intel i5 − 6500 with 3.20GHz) in parallel. In contrast, the same numerical simulation of (2) based on $\mathbf{f}_{\text{ana}}$ runs approximately one hour on the same PC. The relatively short simulation times enable us not only to use integration schemes with smaller numerical truncation error, e.g., spectral methods with ETD2 [86], but also to move the spot along longer, complex trajectories like e.g. the SFB910 curve [SI_video2] or skyline of Berlin [SI_video3].

3.1.1. Stability of position control Open loop controls are independent of the actual controlled system state and are thus unable to take into account unmodeled influences or perturbations. All open loop control method can thus be inherently unstable against perturbations of the initial conditions, data uncertainty, or numerical roundoff errors. However, for protocol velocities $\dot{\mathbf{\Phi}} \sim \mathbf{v}_0$ close to the uncontrolled velocity $\mathbf{v}_0$, the control signal (7) is small in amplitude and enforces a wave profile which is relatively close to the uncontrolled spot profile $\mathbf{U}_c$. Because the latter is presumed to be stable, the controlled spot can in principle benefit from that stability, resulting in a stable open loop control. This expectation has been confirmed numerically [45, 48] and analytically [47] for a variety of controlled RD systems in 1D.

To test the stability of analytical position control $\mathbf{f}_{\text{ana}}$ of two-dimensional spots we accelerate or decelerate a single spot from its initial, intrinsic velocity $\mathbf{v}_0$ to a final velocity $\mathbf{v}_1$ using a translational protocol of motion $\mathbf{\Xi}(t) = (\mathbf{\Phi}, 0)^T$ with velocity

$$\dot{\Phi}_i(t) = \begin{cases} v_0^i, & t < 0, \\ \frac{1}{2}\left((v_0^i + v_1^i) + (v_0^i - v_1^i)\cos\left(\pi t/T_i\right)\right), & 0 \le t \le T_i, \\ v_1^i, & t > T_i, \end{cases} \tag{15}$$

for $i \in \{x, y\}$. Note that both the protocol's velocity $\dot{\mathbf{\Phi}}(t)$ and acceleration $\ddot{\mathbf{\Phi}}(t)$ are continuous function during the interval $[0, T_i]$ where T_i denotes the duration of the protocol. The maximum acceleration $\pi\left(v_i^1 - v_i^0\right)/(2T_i)$ is proportional to the prescribed velocity difference $v_i^1 - v_i^0$ and inversely proportional to T_i. Hence, smoother protocols with $T_i \gg 1$ accelerate the spot less compared to rapid ones with $T_i \ll 1$.

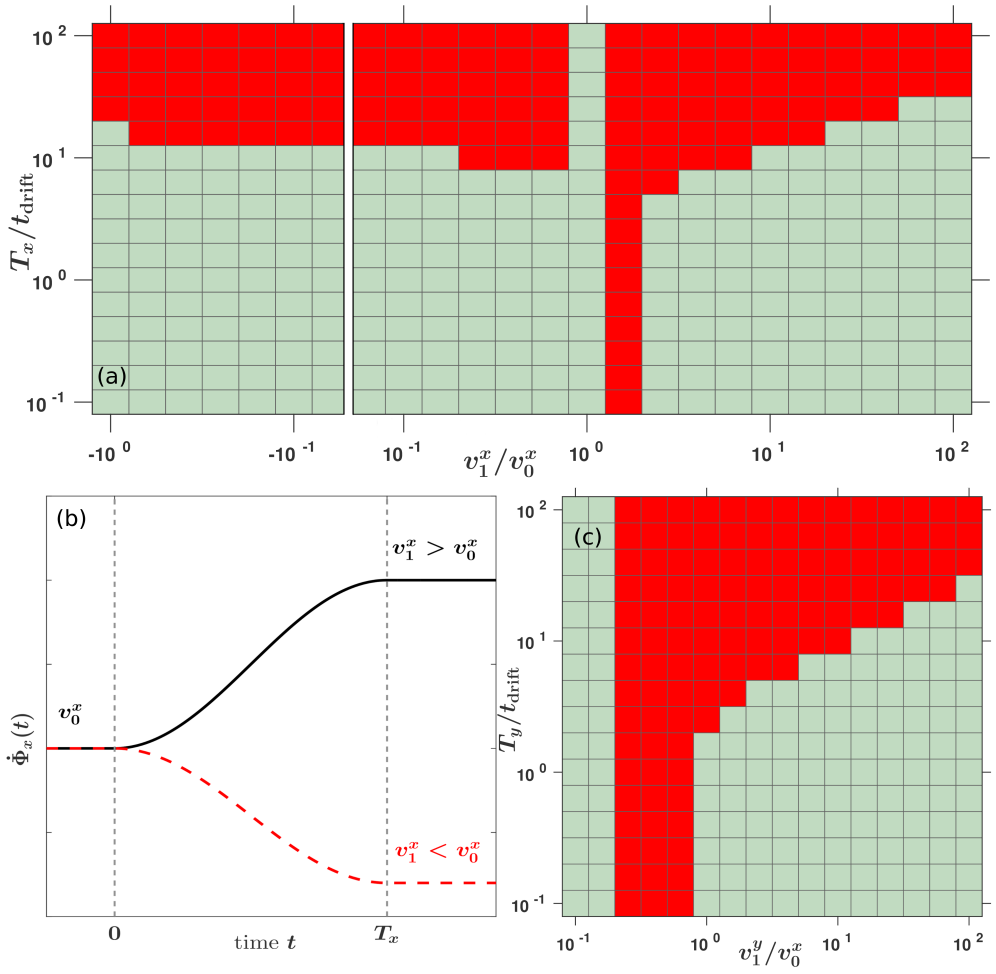

Figure 3. Numerically evaluated region of stability for analytical position control. Stability (green regions) and instability (red regions) is demonstrated for a sinusoidal protocol of motion (15) illustrated in panel (b) which accelerates or decelerates a single spot from its initial, intrinsic velocity $\mathbf{v}_0$ to the final velocity $\mathbf{v}_1$ during the time T_i, $i = \{x, y\}$. In panel (a) the spot is exclusively accelerated or decelerated along its intrinsic direction of motion. In panel (c) the spot keeps moving with its intrinsic velocity along its intrinsic direction of motion while is accelerated or decelerated perpendicular to it. The controlled spot dynamics (1) is simulated on a $(-0.35, 0.35] \times (-0.35, 0.35]$ domain with periodic boundary condition using semi-implicit ETD2 [86] with time step $dt = 0.01$ such that the local numerical truncation error is $< 10^{-4}$. The system parameters coincide with set 1 in table 1 and thus the drift time is given by $t_{\rm drift} = L/v_0^x \approx 273$.

A sketch of the protocol is depicted in figure 3(b). Since the proposed control scheme is an open loop control, deviations between the current spot's position $\mathbf{\Phi}_{\mathrm{curr}}(t)$ and the POM $\mathbf{\Phi}(t)$ will grow unbounded in time if the difference between them exceeds a critical value [47]. A specific protocol is called *stable* and marked by green boxes in figure 3 if and only if the Euclidean distance is bounded as $\|\mathbf{\Phi}_{\mathrm{curr}}(t) - \mathbf{\Phi}(t)\| < L/2$ for all times $t \in [0, t_{\mathrm{end}}]$. Otherwise, it is called *unstable* (red boxes). Note that the protocol is also considered to be unstable if the application of the control signal leads to the creation of further spots. In order to make the results comparable for different protocol durations, we adjust the terminal simulation time t_{end} according to $t_{\mathrm{end}} = \max\left(10\, t_{\mathrm{drift}}, T_i + 10\, L/|v_1^i|\right)$ with drift time $t_{\mathrm{drift}} = L/v_0^x$. We stress that all simulation results presented in figure 3 have been computed for sufficiently long time intervals and do not alter upon an increase of the total simulation time.

Figure 3(a) depicts in green the numerically evaluated region of stability for the POM (15) in x-direction as a function of the ratio of terminal spot velocity v_1^x to the initial one v_0^x and the ratio of the control duration T_x to the drift time $t_{\mathrm{drift}} \equiv L/v_0^x$. The translational POM in y-direction is set to zero, $\Phi_y(t) = 0$. At first glance, one notices that our numerical algorithm is stable in the absence of control, $v_1^x/v_0^x = 1$, regardless of the terminal simulation time $t_{\mathrm{end}} \propto T_x$. Further, it turns out that the control scheme is mostly stable for rapid, $T_x \ll t_{\mathrm{drift}}$, to moderately slow POMs, $T_x \lesssim 10 t_{\mathrm{drift}}$, regardless of the velocity change, $|v_1^x - v_0^x|$. The stability regions exhibit an asymmetry with respect to the sign of the velocity change. Weakly accelerating protocols with $1 < v_1^x/v_0^x \lesssim 2$ are unstable (red colored region) while decelerating protocols with $v_1^x < v_0^x$ are always stable for $T_x \lesssim 10 t_{\mathrm{drift}}$. This finding is in agreement with [47]. The instability for $v_0^x < v_1^x \lesssim 2v_0^x$ is due to an undesired rotation of the spot induced by numerical truncation errors accumulated during the simulation and eventually resulting in an asymmetric perturbation (with respect to y) acting on the spot pattern. Once the spot starts to rotate and eventually drifts away from the centerline $y = 0$, the proposed control $\mathbf{f}_{\mathrm{ana}}$ can neither respond nor correct the undesired rotation due to its open-loop control design. Thus, the distance $\|\mathbf{\Phi}_{\mathrm{curr}}(t) - \mathbf{\Phi}(t)\|$ grows unbounded in time. The impact of numerical truncation error becomes more pronounced with growing protocol's duration T_x and results in a broad unstable region for protocols with long duration, $T_x > 10 t_{\mathrm{drift}}$.

The situation changes if one aims to translate the spot pattern perpendicular to its intrinsic direction of propagation, here in y-direction. Therefore, we keep the motion in x unchanged, $\Phi_x(t) = v_0^x\, t$, and accelerate the spot according to (15) along the y-direction. Because the controlled spot solution is symmetric with respect to the centerline $y = 0$, position control in y might be inherently unstable [47]. One notices immediately that the region where position control is unstable becomes much larger if its applied in y instead of x, compare figure 3(a) and figure 3(c). Nevertheless, the control is stable for weak acceleration, $v_1^y \simeq 0.1 v_0^x$, independent of the protocol's duration. Increasing the terminal velocity further, analytical control starts to fail. Once a certain deviation between the current spots' position and the proposed POM is attained, the pattern cannot follow the applied control anymore and starts to move freely. Often, new spots are created by the continuously acting control. With further growing terminal velocity v_1^y, the control's magnitude increases as well and thus successful position control can be re-stabilized. Longer protocols T_y might result in an accumulating of numerical truncation errors.

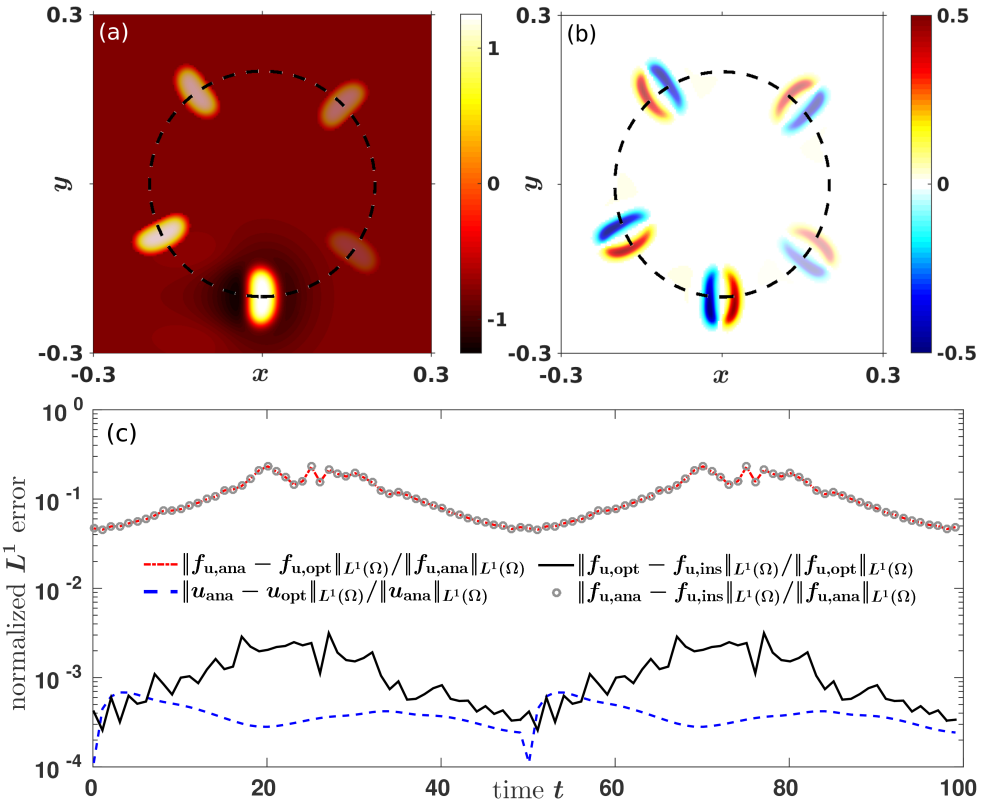

Figure 4. Position control along a circular desired distribution (16) with radius $r = 0.2$ and duration time $T = 200$. (a) Snapshots of the temporal evolution of the activator distribution $u(\mathbf{r}, t)$ obtained from numerical simulation of (1)-(2a) at different instants of time $t = \{30, 75, 120, 165, 200\}$. (b) Distribution of the analytical control signal acting on u, $f_{u,\mathrm{ana}}(\mathbf{r}, t)$, derived from (7) at the same moments. The direction of time evolution is indicated by the decreasing transparency. (c) Temporal evolution of the relative error measured by the $L^1(\Omega)$ norm between the analytical $f_{u,\mathrm{ana}}$, (7), the insert $f_{u,\mathrm{ins}}$, (3), and the optimal control signal $f_{u,\mathrm{opt}}$, (8), acting on activator u in the time horizon $[0, T/2]$. The controlled spot dynamics (1) is simulated on a $(-0.5, 0.5] \times (-0.5, 0.5]$ domain with periodic boundary conditions and an implicit Euler method in time [SI_video4]. The system parameters are the set 1 from table 1.

3.2. Pseudo-orientation control

In the previous paragraph, we demonstrate that the stability of analytical position control can be enhanced if the control signal is primarily acting along the spot's symmetry axis, being determined by the current orientation of the spot pattern $\Phi_\varphi(t)$. Therefore, we propose to translate the spot pattern along a circular trajectory while simultaneously controlling its orientation

$$\dot{\Phi}_x(t) = r \sin\left(\Phi_\varphi(t)\right), \quad \dot{\Phi}_y(t) = -r \cos\left(\Phi_\varphi(t)\right), \quad \Phi_\varphi(t) = 2\pi t/T, \tag{16}$$

in our following example. Here, r denotes the radius of the circle and T the protocol's duration. We stress that to use a protocol where the pattern moves on a circle with large circumference is the easiest consistent and experimentally feasible approach

[29]. In figure 4, we present the temporal evolution of the activator distribution u (panel (a)) controlled by the analytic control $\mathbf{f}_{\text{ana}}$ (panel (b)). As desired, the spot's orientation vector is always tangent to the protocol of motion. Further, the control signals $\mathbf{f}_{\text{ana}}$ remain localized and are dominated by the translational Goldstone modes $\partial_{\xi_x}\mathbf{U}_c$ and $\partial_{\xi_y}\mathbf{U}_c$ due to the relative strong acceleration along $\boldsymbol{\Xi}(t)$ (16); the average speed is $\bar{v} \simeq 2.4 v_x^0$. In panel figure 4 (c), the temporal behavior of the relative error between the analytical control signal $\mathbf{f}_{\text{ana}}$, the insert control $\mathbf{f}_{\text{ins}}$, and the optimal control signal $\mathbf{f}_{\text{opt}}$ measured by the $L^1(\Omega)$ norm are presented. One notices that the relative errors are larger compared to position control along a Lissajous curve, cf. figure 2. These stronger deviations are caused by interpolation errors arising during the numerical rotation of spot patterns by $\Phi_\varphi(t)$. Consequently, the relative error between the analytical and the optimal control signal attains its maximum value of $\sim 25\%$ if $\Phi_\varphi(t) = m\,45°$, m odd. At these angles the distance between the nodes of the rotated grid and the underlying one is the largest, viz., $dx/\sqrt{2}$, and, hence, numerical interpolation errors become significant. Contrary, $\|f_{u,\text{ana}}(t) - f_{u,\text{opt}}(t)\|_{L^1(\Omega)}$ reaches its smallest value of $\sim 5\%$ if $\Phi_\varphi(t) = m\,90°$, $m \in \mathbb{Z}$, at which both grids coincide. Remarkable, the normalized error between the analytically controlled activator trajectory and the optimal one, $\|u_{\text{ana}}(t) - u_{\text{opt}}(t)\|_{L^1(\Omega)}/\|u_{\text{ana}}(t)\|_{L^1(\Omega)}$ (dashed line), is still less than 10^{-3} at any time despite that the deviation of the associated controls rises up to $\sim 25\%$.

3.3. Orientation control

If the traveling wave patterns supposed to be controlled are moving on its own, $\mathbf{v}_0 \neq \mathbf{0}$, the simplest way to guide them in space is to control exclusively its current orientation $\Phi_\varphi(t)$. If so, the translational components of the POM $\boldsymbol{\Xi}(t)$ are determined by

$$\dot{\Phi}_x(t) = v_0^x \cos\left(\Phi_\varphi(t)\right), \quad \dot{\Phi}_y(t) = v_0^x \sin\left(\Phi_\varphi(t)\right). \tag{17}$$

Clearly, one loses the possibility to control separately the x- and y-position of the pattern by limiting the speed to $\|\dot{\boldsymbol{\Phi}}(t)\| = v_0^x$. Inserting (17) into (7), the analytical control signals simplify significantly and are solely determined by the rotational Goldstone modes

$$\mathbf{f}_{\text{ana}}(\mathbf{r}, t) = -\dot{\Phi}_\varphi(t)\partial_\varphi \mathbf{U}_c(\mathbb{A}(-\Phi_\varphi(t))\,(\mathbf{r} - \boldsymbol{\Phi}(t))), \quad \text{with}\, \omega_0 = 0. \tag{18}$$

In our next example, we pick up the initial problem from section 1, namely, how to prevent pinning of spots at local heterogeneities in the medium. The heterogeneity is realized by a circular defect of jump type in the additive parameter κ_1, i.e., the value of κ_1 changes from the background value κ_1^{back}, $\forall \mathbf{r} \notin \Omega_\circ$, to κ_1^{het}, $\forall \mathbf{r} \in \Omega_\circ$, inside the heterogeneity with $\Omega_\circ = \{(x, y) \in \mathbb{R}^2 : (x + R)^2 + y^2 < R^2\}$ with radius $R = 0.05$. The orientational POM for avoiding the heterogeneity is set to

$$\Phi_\varphi(t) = \frac{\pi}{4} \sin\left(\frac{2\pi t}{T}\right), \tag{19}$$

with duration $T = L_x/v_0^x$. Note that the corresponding prescribed positions $(\Phi_x(t), \Phi_y(t))^T$ have to be calculated numerically.

In figure 5, we present the temporal evolution of the activator distribution u obtained from numerical simulation of (1)-(2a) with $\mathbf{f}_{\text{ana}}$, (18), in panel (a) and

the corresponding control signal $f_{u,\mathrm{ana}}$ in panel (b). The presumed translational POM is indicated by the dashed lines. At first glance, one notices that the control signal possesses a more complicated shape and its magnitude is significantly reduced, $|f_{u,\mathrm{ana}}| \lesssim 10^{-3}$, compared to $|f_{u,\mathrm{ana}}| \lesssim 10^{0}$ and $|f_{u,\mathrm{ana}}| \lesssim 10^{-1}$ for the previous examples, cf. figure 2 and figure 4, respectively. Thus, orientational control is a less invasive scheme to avoid the collision with defects compared to position control. The price one pays is to lose the ability to react fast and rapidly shift the spot. Additionally, orientation control is much more susceptible to failure due to the small control magnitudes. The latter are too weak to suppress the impact of numerical roundoff errors resulting in an undesired rotation of the spot, cf. section 3.1.1. Caused by the small propagation velocity, the duration of the protocol of motion T grows compared with position control, see section 3.1, and therefore the probability of failure increases as well. Moreover, the numerical calculation of optimal control (8) is hardly accessible due to the long duration $T \simeq 563$ as well as the weak magnitudes and, thus, preventing a comparison between analytical and optimal control.

3.4. Position control by a single control signal

So far only examples of fully actuated systems have been discussed for which the number of state components equals the number independent of control signals. If the coupling matrix $\mathbb{B}$ is not invertible, the expression for $\mathbf{f}_{\mathrm{ana}}$, (7), cannot be used, and the question arises how the proposed analytical control approach can be extended to underactuated systems [45, 80]. Here, we discuss the case of a single control signal applied to a system with multiple components. For simplicity, we assume a control acting on the activator u only and both inhibitors v and w remain uncontrolled, i.e., $f_{v,\mathrm{ana}}(\mathbf{r},t) = f_{w,\mathrm{ana}}(\mathbf{r},t) = 0$. Control via an inhibitor is also possible and has been discussed in detail for the Hodgkin-Huxley model and the three-component Oregonator model for photosensitive BZ reaction in the supplemental information to [45]. In order to derive an expression for the analytical control signal, we initially write down a system with a control $\mathbf{f}$ acting on each component

$$\partial_t u(\mathbf{r},t) = D_u \Delta u + \kappa_2\, u - u^3 - \kappa_3 v - \kappa_4 w + \kappa_1 + f_u, \tag{20a}$$

$$\tau \partial_t v(\mathbf{r},t) = D_v \Delta v + u - v + f_v, \tag{20b}$$

$$\theta \partial_t w(\mathbf{r},t) = D_w \Delta w + u - w + f_w. \tag{20c}$$

Both inhibitor kinetics (20b)-(20c) can be viewed as linear, inhomogeneous PDEs with initial conditions $v(\mathbf{r},t_0) = v_0(\mathbf{r})$ and $w(\mathbf{r},t_0) = w_0(\mathbf{r})$, respectively. Their solutions can be written as

$$\tilde{v}(\mathbf{r},t) = \mathcal{K}_v^0 \circ v_0 + \frac{1}{\tau}\mathcal{K}_v \circ (u + f_v)\,, \quad \tilde{w}(\mathbf{r},t) = \mathcal{K}_w^0 \circ w_0 + \frac{1}{\theta}\mathcal{K}_w \circ (u + f_w)\,, \tag{21}$$

where $\mathcal{K}_i^0$ and $\mathcal{K}_i$, $i \in \{v, w\}$, are integral operators, involving Green's functions to the homogeneous equations of (20b)-(20c) with associated initial conditions and to the inhomogeneous equations with zero initial conditions. Plugging (21) into (20a), one gets

$$\begin{aligned}\partial_t u(\mathbf{r},t) = {} & D_u \Delta u + \kappa_2\, u - u^3 - \kappa_3 \left[\mathcal{K}_v^0 \circ v_0 + \frac{1}{\tau}\mathcal{K}_v \circ u\right] - \kappa_4 \left[\mathcal{K}_w^0 \circ w_0 + \frac{1}{\theta}\mathcal{K}_w \circ u\right] + \kappa_1 \\ & + f_u - \frac{\kappa_3}{\tau}\mathcal{K}_v \circ f_v - \frac{\kappa_4}{\theta}\mathcal{K}_w \circ f_w.\end{aligned} \tag{22}$$

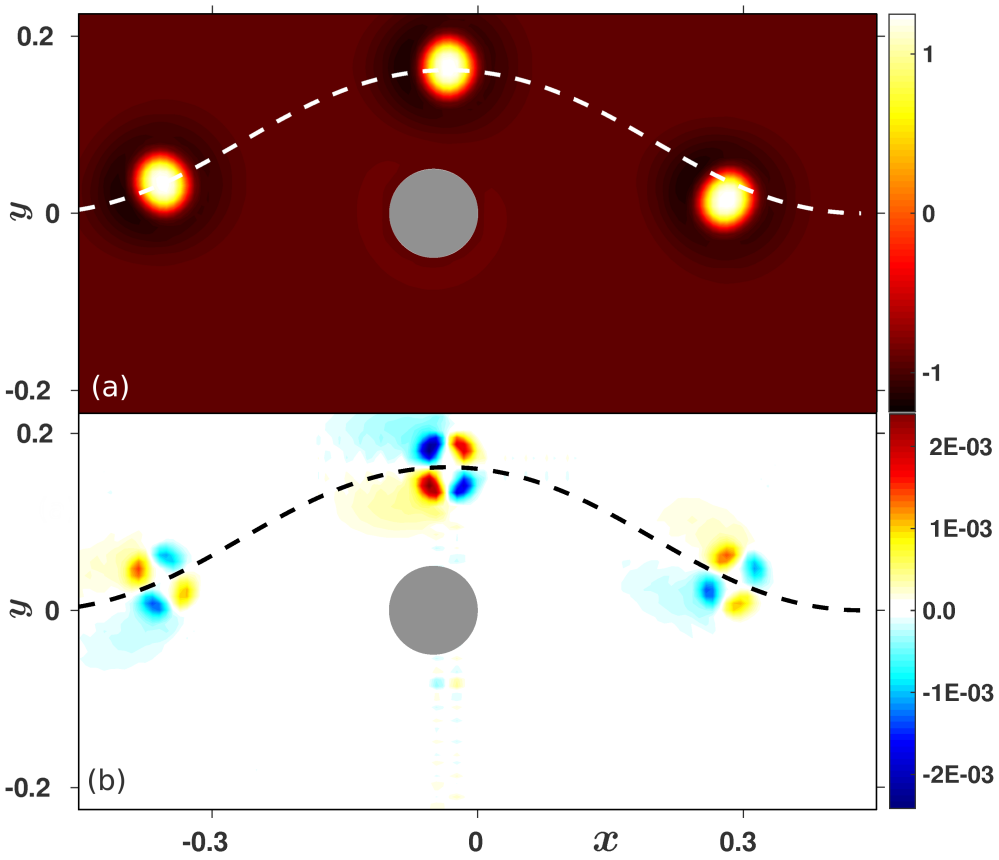

Figure 5. Orientation control to avoid collision with circular heterogeneity [SI_video5]. Time evolution of activator distribution u (top panel (a)) obtained from numerical simulation of (1)-(2a) with $\mathbf{f}_{\text{ana}}$, (18), at different instants of time $t = \{100, 250, 400\}$ and the corresponding distribution of $f_{u,\text{ana}}$ (bottom panel (b)) are shown. The decreasing transparency indicates consecutive instants of time. The controlled spot dynamics is simulated on a $(-0.5, 0.5] \times (-0.25, 0.25]$ domain with periodic boundary condition using ETD2 in time. We use the parameter set 2 in table 1 and the circular defect with radius $R = 0.05$ is modeled by a jump in κ_1 from its background value of $\kappa_1^{\text{back}} = -7.30$ to the value inside the heterogeneity $\kappa_1^{\text{het}} = -7.50$.

From the last line of (22), we identify the expression for the analytical control $f_{u,\text{ana}}^{\text{sing}}$ acting exclusively on the activator equation

$$f_{u,\text{ana}}^{\text{sing}}(\mathbf{r}, t) = f_{u,\text{ana}}(\mathbf{r}, \mathbf{t}) - \frac{\kappa_3}{\tau}\mathcal{K}_v \circ f_{v,\text{ana}} - \frac{\kappa_4}{\theta}\mathcal{K}_w \circ f_{w,\text{ana}}, \tag{23}$$

whereby the component of the analytical control signal $\mathbf{f}_{\text{ana}}$ are determined by (7). As an example for position control by a single control signal, we guide a spot along the Lissajous curve, (13), with radius $r = 0.2$ and protocol duration $T = 200$. The spot's orientation $\Phi_\varphi(t) = 0$ remains uncontrolled. The temporal behavior of the relative errors as measured by the $L^1(\Omega)$ norm (14) between desired and controlled states obtained from numerical simulation of (1)-(2a) with control $\mathbf{f}_{\text{ana}}^{\text{sing}} = (f_{u,\text{ana}}^{\text{sing}}, 0, 0)^T$ given by (23) are presented in figure 6(c). At a first glance, one notices that the

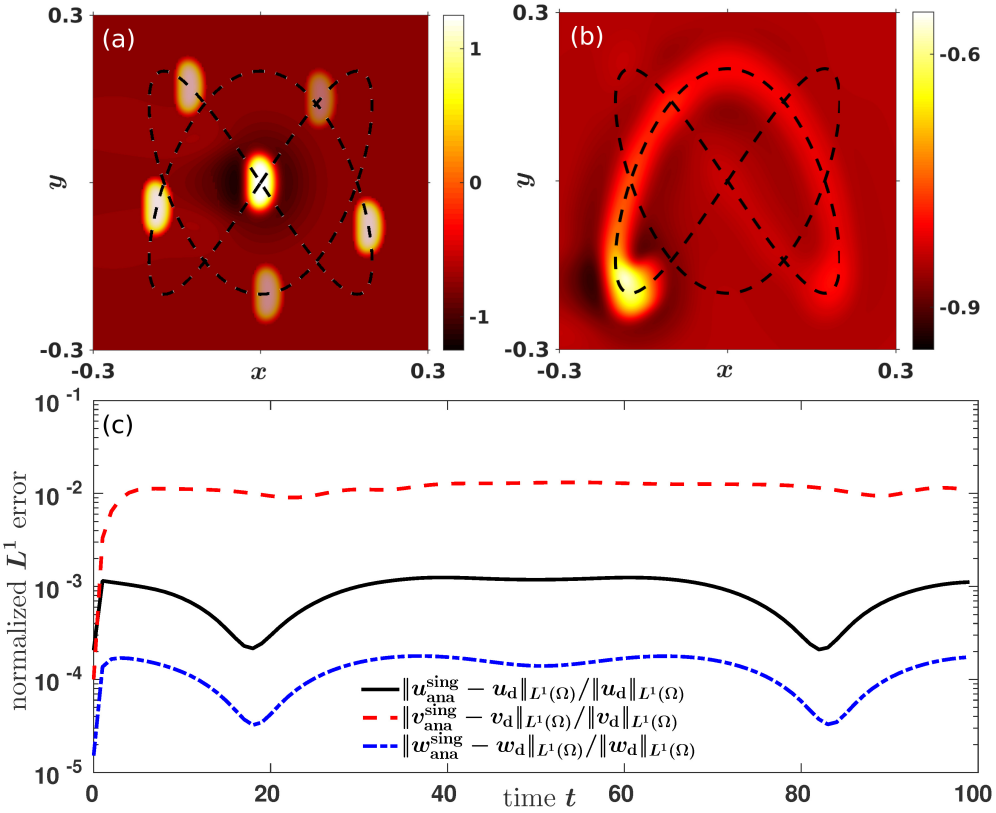

Figure 6. Position control by a single control signal acting on the activator u along the Lissajous curve (13) with radius $r = 0.2$ and protocol duration $T = 200$. (a) Time evolution of activator distribution u obtained from numerical simulation of (1)-(2a) with $\mathbf{f}_{\rm ana}^{\rm sing} = (f_{u,\rm ana}^{\rm sing}, 0, 0)^T$, (23), at different instants of time $t = \{10, 50, 90, 130, 170, 200\}$. The decreasing transparency marks consecutive instants of time. (b) Distribution of the inhibitor v at $t = 180$. (c) Temporal behavior of the relative error as measured by the $L^1(\Omega)$ norm (14), between the numerical obtained states and the desired distribution $\mathbf{U}_d$ during $t \in [0, T/2]$. The controlled spot dynamics is simulated on a $(-0.5, 0.5] \times (-0.5, 0.5]$ domain with periodic boundary conditions using ETD2 in time [SI_video6]. We use set 1 in table 1 as system parameters.

relative error for the activator u (solid line) is less than 10^{-3} at any time t and thus the controlled activator agrees satisfactorily well with the desired distribution. This finding is corroborated by snapshots of u at different instants of time in figure 6(a). In contrast to the activator profile, the distribution of the inhibitor v is not preserved and deformed drastically, see figure 6(b). In particular, one recognizes an elongated region of activity along the Lissajous curve due to the presumed time scale separation in the RDS (1). Any local production of the slow inhibitor v caused by the presence of u, (20b), decays exponentially to the homogeneous rest state on the time scale $\tau = 48 \approx T/4$. Consequently, the relative error of v (dashed line) attains relatively large values of 10^{-2}. On the other hand, the fast inhibitor w possesses the same time scale parameter as u, namely $\theta = 1$, and therefore its profile is largely preserved. In

fact, the relative error for w attains values of less than 10^{-4} and thus is even one magnitude smaller than the relative error of u, cf. the dash-dotted line in figure 6(c).

4. Conclusion

The ability to control both the position and the orientation of a desired traveling wave solution according to a prescribed trajectory in space has attracted considerable attention over the last decades and it is still a fundamental problem in applied nonlinear science. In this work, we have extended our recently proposed analytic method for position control of fully actuated reaction-diffusion systems in one spatial dimension [45, 80] to spatially localized moving patterns – also called dissipative solitons or shortly spots – in a two-dimensional spatial domain. The derived position control is realized by external spatio-temporal forcing, i.e., it is an open-loop control. Intriguingly, no detailed knowledge about the underlying systems dynamics and, especially, about the exact reaction kinetics is needed in contrast to usual open-loop controls. Additionally, it is designed to preserve simultaneously the shape of the controlled pattern and it can be pre-computed once the intrinsic propagation velocity and the profile of the uncontrolled spot have been measured with sufficient accuracy. Consequently, a continuous recording of the system is not necessary in contrast to closed-loop or feedback control loops. Remarkably, it turns out that the analytical position controls are solutions to the unregularized optimal control problem. Hence, we have also compared the analytic control signals with regularized optimal control with help of numerical examples using a three component reaction-diffusion system as a spot forming system.

In a first example, we have studied the ability of position control without orientation control. It turns out that the states controlled by analytic control as well as optimal control agree remarkably well along the trajectory and, in particular, the relative error between the desired distribution and the state solutions is negligible small. Further, we have confirmed, within numerical accuracy, that the analytical position control is indeed the solution to an unregularized optimal control problem and even close to the regularized one. Consequently, they are an excellent initial guesses for the numerical calculation of regularized optimal control problems with small regularization parameter, thereby achieving a substantial computational speedup. Generally, the analytical expressions may serve as consistency checks for numerical optimal control algorithms as well.

To test the robustness of our analytical position control in 2D, we have performed numerical stability tests in section 3.1.1. It is found that the control scheme is mostly stable if the spot is accelerated or decelerated in direction of its intrinsic propagation. Thereby, the region of stability exhibits an asymmetry with respect to the sign of the velocity change caused by the broken mirror symmetry of the spot profile. If one guides the spot perpendicular to its intrinsic direction of propagation, position control might be inherently unstable due the spots symmetry with respect to the centerline [47]. Indeed, the parameter region of stable protocols of motion shrinks drastically. Nevertheless, our position control is stable for weak accelerations as well as very strong ones. In general, longer protocol durations result in an accumulating of numerical truncation errors and hence decreases the stability of control. The latter can be re-enforced e.g. by an additional non-invasive feedback control computed for the system linearized around the desired distribution [87].

Because spots are moving on its own, the simplest way to guide them in space is

to control exclusively its orientation. Thereby, the derived magnitude of orientational control is significantly reduced by several orders of magnitude. Hence, orientational control is a less invasive scheme. The price one pays is to lose the ability to react fast and rapidly shift the spot. Additionally, orientation control is much more susceptible to failure due to the small control magnitudes.

First and foremost, the assumption of fully actuated reaction-diffusion systems is overly restrictive in applications of our proposed position control scheme. Usually, the number of state components is larger than the amount of control signals, and introducing additional means of spatio-temporal control to increase the number of independent control signals is often not feasible. Although the analytic approach can be extended to underactuated systems by entailing additional assumptions about the desired distribution, this usually leads to control signals which strongly deform the wave profile for some state components, see section 3.4. While this restriction cannot be treated within the analytical approach in general, optimal control works for underactuated systems as well.

Finally, we stress that the presented approach to position control is not limited to traveling or stationary spot solutions in reaction-diffusion systems. It can be extended to other traveling waves solutions in reaction-diffusion systems as e.g. rigidly rotating spiral waves in two and scroll waves in three dimensions. Furthermore, the approach is not at all restricted to evolution equations of reaction-diffusion type but also applies to e.g. nonlocal integro partial differential equations which exhibit localized bump solutions similar to spots in reaction-diffusion systems [82, 83].

Acknowledgments

We acknowledge financial support from the German Science Foundation DFG through the SFB 910 “Control of Self-Organizing Nonlinear Systems”.

[1] Kapral R and Showalter K (eds) 1995 *Chemical Waves and Patterns* (Kluwer, Dordrecht)
[2] Koch C and Segev I 2000 *Nat. Neurosci.* **3**
[3] Zipes D P and Jalife J (eds) 2014 *Cardiac Electrophysiology: from Cell to Bedside* 6th ed (W.B. Saunders, Philadelphia)
[4] Bailey N T J 1975 *The Mathematical Theory of Infectious Diseases and its Applications* (Charles Griffin & company ltd)
[5] Bement W M, Leda M, Moe A, Kita A, Larson M, Golding A, Pfeuti C, Su K C, Miller A, Goryachev A and vonDassow G 2015 *Nat. Cell Biol.* **17** 1471–1483 ISSN 1465-7392, 1476-4679 URL `http://www.nature.com/doifinder/10.1038/ncb3251`
[6] Löber J, Ziebert F and Aranson I S 2014 *Soft Matter* **10**(9) 1365–1373 URL `http://dx.doi.org/10.1039/C3SM51597D`
[7] Radszuweit M, Alonso S, Engel H and Bär M 2013 *Phys. Rev. Lett.* **110**(13)
[8] Kulawiak D A, Camley B A and Rappel W J 2016 *PLOS Comput. Biol.* **12** URL `http://dx.doi.org/10.1371%2Fjournal.pcbi.1005239`
[9] Cross M and Hohenberg P 1993 *Rev. Mod. Phys.* **65**
[10] Hagberg A and Meron E 1994 *Phys. Rev. Lett.s* **72** 2494 URL `https://doi.org/10.1103/PhysRevLett.72.2494`
[11] Mikhailov A and Showalter K 2006 *Phys. Rep.* **425** 79–194
[12] Vanag V K and Epstein I R 2008 *Chaos* **18** 026107 URL `http://scitation.aip.org/content/aip/journal/chaos/18/2/10.1063/1.2900555`
[13] Pierre T, Bonhomme G and Atipo A 1996 *Phys. Rev. Lett.* **76** 2290–2293 URL `http://link.aps.org/doi/10.1103/PhysRevLett.76.2290`
[14] Lüthje O, Wolff S and Pfister G 2001 *Phys. Rev. Lett.* **86** 1745–1748 URL `http://link.aps.org/doi/10.1103/PhysRevLett.86.1745`
[15] Kim M, Bertram M, Pollmann M, von Oertzen A, Mikhailov A S, Rotermund H H and Ertl G 2001 *Science* **292** 1357

[16] Zykov V S, Bordiougov G, Brandtstädter H, Gerdes I and Engel H 2003 *Phys. Rev. E* **68** 016214 URL http://link.aps.org/doi/10.1103/PhysRevE.68.016214
[17] Chen J X, Zhang H and Li Y Q 2009 *J. Chem. Phys.* **130** 124510 URL http://scitation.aip.org/content/aip/journal/jcp/130/12/10.1063/1.3098543
[18] Lou Y and Christofides P D 2003 *IEEE Trans. Control Syst. Tech.* **11** ISSN 1063-6536
[19] Gomes S N, Pradas M, Kalliadasis S, Papageorgiou D T and Pavliotis G A 2015 *Phys. Rev. E* **92** 022912 URL http://link.aps.org/doi/10.1103/PhysRevE.92.022912
[20] Hoffmann K H, Leugering G and Tröltzsch F (eds) 1998 *Optimal Control of Partial Differential Equations* (*ISNM* vol 133) (Birkhäuser Verlag)
[21] Hoffmann K H, Lasiecka I, Leugering G, Sprekels J and Tröltzsch F (eds) 2002 *Optimal Control of Complex Structures* (*ISNM* vol 139) (Birkhäuser Verlag)
[22] Barthel W, John C and Tröltzsch F 2010 *Z. Angew. Math. und Mech.* **90** 966–982
[23] Martens S, Löber J and Engel H 2015 *Phys. Rev. E* **91** 022902 URL http://link.aps.org/doi/10.1103/PhysRevE.91.022902
[24] Zheng Z, Kim H and Stone H A 2015 *Phys. Rev. Lett.* **115** ISSN 0031-9007, 1079-7114 URL http://link.aps.org/doi/10.1103/PhysRevLett.115.174501
[25] Ziepke A, Martens S and Engel H 2016 *J. Chem. Phys.* **145** 094108 ISSN 0021-9606 URL http://aip.scitation.org/doi/abs/10.1063/1.4962173
[26] Haas G, Bär M, Kevrekidis I G, Rasmussen P B, Rotermund H H and Ertl G 1995 *Phys. Rev. Lett.* **75** 3560
[27] Schlesner J, Zykov V S, Brandtstädter H, Gerdes I and Engel H 2008 *New J. Phys.* **10** 015003
[28] Wolff J, Papathanasiou A G, Rotermund H H, Ertl G, Li X and Kevrekidis I G 2003 *Phys. Rev. Lett.* **90** 018302 URL http://link.aps.org/doi/10.1103/PhysRevLett.90.018302
[29] Qiao L, Li X, Kevrekidis I G, Punckt C and Rotermund H H 2008 *Phys. Rev. E* **77** 036214 URL http://link.aps.org/doi/10.1103/PhysRevE.77.036214
[30] Steinbock O, Zykov V S and Müller S C 1993 *Nature* **366** 322–324
[31] Schrader A, Braune M and Engel H 1995 *Phys. Rev. E* **52** 98
[32] Odent V, Louvergneaux E, Clerc M G and Andrade-Silva I 2016 *Phys. Rev. E* **94** 052220 URL http://link.aps.org/doi/10.1103/PhysRevE.94.052220
[33] Kevrekidis P G, Kevrekidis I G, Malomed B A, Nistazakis H E and Frantzeskakis D J 2004 *Phys. Scr.* **69** 451 URL http://stacks.iop.org/1402-4896/69/i=6/a=003
[34] Zykov V S, Bordiougov G, Brandtstädter H, Gerdes I and Engel H 2004 *Phys. Rev. Lett.* **92** 018304 URL http://link.aps.org/doi/10.1103/PhysRevLett.92.018304
[35] Schlesner J, Zykov V and Engel H 2008 *Feedback-mediated Control of Hypermeandering Spiral Waves* (Wiley-VCH Verlag) pp 591–607 ISBN 9783527622313 URL http://dx.doi.org/10.1002/9783527622313.ch27
[36] Sakurai T, Mihaliuk E, Chirila F and Showalter K 2002 *Science* **296** 2009–2012
[37] Dahms T, Hövel P and Schöll E 2007 *Phys. Rev. E* **76** 056201 URL http://link.aps.org/doi/10.1103/PhysRevE.76.056201
[38] Mihaliuk E, Sakurai T, Chirila F and Showalter K 2002 *Phys. Rev. E* **65** 065602 URL http://link.aps.org/doi/10.1103/PhysRevE.65.065602
[39] Schlesner J, Zykov V S, Engel H and Schöll E 2006 *Phys. Rev. E* **74** 046215 URL http://link.aps.org/doi/10.1103/PhysRevE.74.046215
[40] Gurevich S V and Friedrich R 2013 *Physical Review Letters* **110** URL http://link.aps.org/doi/10.1103/PhysRevLett.110.014101
[41] Vladimirov A G, Pimenov A, Gurevich S V, Panajotov K, Averlant E and Tlidi M 2014 *Phil. Trans. R. Soc. A* **372** 20140013 ISSN 1364-503X, 1471-2962 URL http://rsta.royalsocietypublishing.org/content/372/2027/20140013
[42] Buchholz R, Engel H, Kammann E and Tröltzsch F 2013 *Comput. Optim. Appl.* **56** 153–185
[43] Casas E, Ryll C and Tröltzsch F 2013 *Comp. Meth. Appl. Math.* **13** 415–442
[44] Bellman R 2003 *Dynamic Programming* Dover Books on Computer Science Series (Dover Publications) ISBN 9780486428093 URL https://books.google.de/books?id=fyVtp3EMxasC
[45] Löber J and Engel H 2014 *Phys. Rev. Lett.* **112** 148305
[46] Ryll C, Löber J, Martens S, Engel H and Tröltzsch F 2016 *Control of Self-Organizing Nonlinear Systems* (Springer International Publishing) chap Analytical, Optimal, and Sparse Optimal Control of Traveling Wave Solutions to Reaction-Diffusion Systems, pp 189–210 ISBN 978-3-319-28028-8 URL http://dx.doi.org/10.1007/978-3-319-28028-8_10
[47] Löber J 2014 *Phys. Rev. E* **89** 062904
[48] Löber J, Martens S and Engel H 2014 *Phys. Rev. E* **90** 062911
[49] Löber J, Coles R, Siebert J, Engel H and Schöll E 2015 Control of chemical wave propagation *Engineering of Chemical Complexity II* ed Mikhailov A and Ertl G (Singapore: World

Scientific)
[50] Purwins H G, Bödeker H U and Liehr A W 2005 Dissipative solitons in reaction-diffusion systems *Dissipative solitons* (Springer) pp 267–308 URL http://link.springer.com/chapter/10.1007/10928028_11
[51] Arecchi F T, Boccaletti S and Ramazza P 1999 *Phys. Rep.* **318** 1–83 ISSN 0370-1573 URL http://www.sciencedirect.com/science/article/pii/S0370157399000071
[52] Le Goff T, Liebchen B and Marenduzzo D 2016 *Phys. Rev. Lett.* **117** 238002 URL http://link.aps.org/doi/10.1103/PhysRevLett.117.238002
[53] Taube J S and Bassett J P 2003 *Cereb. Cortex* **13** 1162–1172 ISSN 1047-3211, 1460-2199 URL http://cercor.oxfordjournals.org/content/13/11/1162
[54] Gilad E, von Hardenberg J, Provenzale A, Shachak M and Meron E 2004 *Phys. Rev. Lett.* **93** URL http://link.aps.org/doi/10.1103/PhysRevLett.93.098105
[55] Barland S, Tredicce J R, Brambilla M, Lugiato L A, Balle S, Giudici M, Maggipinto T, Spinelli L, Tissoni G, Kndl T, Miller M and Jger R 2002 *Nature* **419** 699–702 ISSN 0028-0836 URL http://www.nature.com/nature/journal/v419/n6908/abs/nature01049.html
[56] Kaminaga A, Vanag V K and Epstein I R 2006 *Angew. Chem., Int. Ed.* **45** 3087–3089 ISSN 1521-3773 URL http://dx.doi.org/10.1002/anie.200600400
[57] Vanag V K and Epstein I R 2007 *Chaos: An Interdisciplinary Journal of Nonlinear Science* **17** 037110 URL http://scitation.aip.org/content/aip/journal/chaos/17/3/10.1063/1.2752494
[58] Tlidi M, Staliunas K, Panajotov K, Vladimirov A G and Clerc M G 2014 *Phil. Trans. R. Soc. A* **372** 20140101 ISSN 1364-503X, 1471-2962 URL http://rsta.royalsocietypublishing.org/content/372/2027/20140101
[59] Schenk C P, Or-Guil M, Bode M and Purwins H G 1997 *Phys. Rev. Lett.* **78** 3781–3784 URL http://link.aps.org/doi/10.1103/PhysRevLett.78.3781
[60] Nishiura Y, Teramoto T and Ueda K I 2005 *Chaos* **15** 047509
[61] FitzHugh R 1961 *Biophys. J.* **1** 445–466
[62] Nagumo J, Arimoto S and Yoshizawa S 1962 *Proc. IRE* **50** 2061–2070
[63] Tarama M, Ohta T and Pismen L M 2011 *Phys. Rev. E* **83**(1) 017201 URL http://link.aps.org/doi/10.1103/PhysRevE.83.017201
[64] Krischer K and Mikhailov A 1994 *Phys. Rev. Lett.* **73** 3165 URL http://journals.aps.org/prl/optabstract/10.1103/PhysRevLett.73.3165
[65] Schimansky-Geier L, Zülicke C and Schöll E 1991 *Zeitschrift für Physik B Condensed Matter* **84** 433–441 URL http://dx.doi.org/10.1007/BF01314019
[66] Doelman A, van Heijster P and Kaper T J 2009 *Journal of Dynamics and Differential Equations* **21** 73–115 URL http://link.springer.com/10.1007/s10884-008-9125-2
[67] van Heijster P, Doelman A and Kaper T J 2008 *Physica D: Nonlinear Phenomena* **237** 3335–3368 URL http://linkinghub.elsevier.com/retrieve/pii/S0167278908002923
[68] Nishiura Y, Teramoto T and Yuan X 2011 *Communications on Pure and Applied Analysis* **11** 307–338 URL http://www.aimsciences.org/journals/displayArticlesnew.jsp?paperID=6492
[69] Yuan X, Teramoto T and Nishiura Y 2007 *Phys. Rev. E* **75** 036220 URL http://link.aps.org/doi/10.1103/PhysRevE.75.036220
[70] Gurevich S V, Amiranashvili S and Purwins H G 2006 *Physical Review E* **74** 066201 URL http://link.aps.org/doi/10.1103/PhysRevE.74.066201
[71] Yang L, Zhabotinsky A M and Epstein I R 2006 *Phys. Chem. Chem. Phys.* **8** 4647–4651 URL http://xlink.rsc.org/?DOI=B609214D
[72] Heidemann G, Bode M and Purwins H G 1993 *Physics Letters A* **177** 225–230 URL http://www.sciencedirect.com/science/article/pii/0375960193900304
[73] Alonso S, John K and Bär M 2011 *The Journal of Chemical Physics* **134** 094117 URL http://scitation.aip.org/content/aip/journal/jcp/134/9/10.1063/1.3559154
[74] Krischer K, Eiswirth M and Ertl G 1992 *The Journal of Chemical Physics* **96** 9161–9172 URL http://scitation.aip.org/content/aip/journal/jcp/96/12/10.1063/1.462226
[75] Lobanova E S and Ataullakhanov F I 2003 *Physical Review Letters* **91** URL http://link.aps.org/doi/10.1103/PhysRevLett.91.138301
[76] Aranson I, Levine H and Tsimring L 1996 *Phys. Rev. Lett.* **76**(7) 1170–1173 URL http://link.aps.org/doi/10.1103/PhysRevLett.76.1170
[77] Xin J 2000 *SIAM Review* **42** 161–230
[78] van Heijster P, Doelman A, Kaper T J, Nishiura Y and Ueda K I 2011 *Nonlinearity* **24** 127–157 URL http://stacks.iop.org/0951-7715/24/i=1/a=007?key=crossref.4e0efc02549da5f41af5674054b591c4

[79] Marwaha B and Luss D 2003 *Chemical Engineering Science* **58** 733–738 URL http://linkinghub.elsevier.com/retrieve/pii/S0009250902006024
[80] Löber J 2017 *Control of Reaction-Diffusion Systems* (Cham: Springer International Publishing) pp 195–220 ISBN 978-3-319-46574-6 URL http://dx.doi.org/10.1007/978-3-319-46574-6_5
[81] Mikhailov A, Schimansky-Geier L and Ebeling W 1983 *Phys. Lett. A* **96** 453–456
[82] Bressloff P C 2012 *J. Phys. A: Math. Theor.* **45** 033001 ISSN 1751-8113, 1751-8121 URL http://stacks.iop.org/1751-8121/45/i=3/a=033001?key=crossref.002dc06e3105150736d5e959fecfd4d8
[83] Coombes S, beim Graben P, Potthast R and Wright J 2014 *Neural Fields* (Springer-Verlag Berlin Heidelberg) ISBN 978-3-642-54593-1
[84] Deisseroth K 2011 *Nature Methods* **8** 26–29 URL http://www.nature.com/doifinder/10.1038/nmeth.f.324
[85] Casas E, Mateos M and Rösch A 2016 *submitted to AIMS Journals*
[86] Cox S M and Matthews P C 2002 *J. Comp. Phys.* **176** 430–455 URL http://www.sciencedirect.com/science/article/pii/S0021999102969950
[87] Bryson A E 1975 *Applied optimal control: optimization, estimation and control* (CRC Press)